The interaction of moist convection and mid-level dry air in the advance of the onset of the Indian monsoon

Parker, D. J., Willetts, P., Birch, C., Turner, A. G. ORCID: https://orcid.org/0000-0002-0642-6876, Marsham, J. H., Taylor, C. M., Kolusu, S. and Martin, G. M. (2016) The interaction of moist convection and mid-level dry air in the advance of the onset of the Indian monsoon. Quarterly Journal of the Royal Meteorological Society, 142 (699). pp. 2256-2272. ISSN 1477-870X doi: 10.1002/qj.2815 Available at https://centaur.reading.ac.uk/43259/

RMetS
Royal Meteorological Society

The interaction of moist convection and mid-level dry air in the advance of the onset of the Indian monsoon

Douglas J. Parker,[a,b*] Peter Willetts,[a] Cathryn Birch,[a,b] Andrew G. Turner,[c,d] John H. Marsham,[a,e] Christopher M. Taylor,[f,g] Seshagirirao Kolusu[a] and Gill M. Martin[b]

[a]*School of Earth and Environment, University of Leeds, UK*
[b]*Met Office, Exeter, UK*
[c]*Department of Meteorology, University of Reading, UK*
[d]*NCAS-Climate, Reading, UK*
[e]*NCAS Atmospheric Physics, Leeds, UK*
[f]*Centre for Ecology and Hydrology, Wallingford, UK*
[g]*National Centre for Earth Observations, Wallingford, UK*

*Correspondence to: D. J. Parker, School of Earth and Environment, University of Leeds, Leeds, LS2 9JT, UK.
E-mail: d.j.parker@leeds.ac.uk

The advance of the onset of the Indian monsoon is here explained in terms of a balance between the low-level monsoon flow and an overrunning intrusion of mid-tropospheric dry air. The monsoon advances, over a period of about 6 weeks, from the south of the country to the northwest. Given that the low-level monsoon winds are westerly or southwesterly, and the mid-level winds northwesterly, the monsoon onset propagates upwind relative to mid-level flow, and perpendicular to the low-level flow, and is not directly caused by moisture flux toward the northwest. Lacking a conceptual model for the advance means that it has been hard to understand and correct known biases in weather and climate prediction models.

The mid-level northwesterlies form a wedge of dry air that is deep in the far northwest of India and over-runs the monsoon flow. The dry layer is moistened from below by shallow cumulus and congestus clouds, so that the profile becomes much closer to moist adiabatic, and the dry layer is much shallower in the vertical, toward the southeast of India. The profiles associated with this dry air show how the most favourable environment for deep convection occurs in the south, and onset occurs here first.

As the onset advances across India, the advection of moisture from the Arabian Sea becomes stronger, and the mid-level dry air is increasingly moistened from below. This increased moistening makes the wedge of dry air shallower throughout its horizontal extent, and forces the northern limit of moist convection to move toward the northwest. Wetting of the land surface by rainfall will further reinforce the north-westward progression, by sustaining the supply of boundary-layer moisture and shallow cumulus. The local advance of the monsoon onset is coincident with weakening of the mid-level northwesterlies, and therefore weakened mid-level dry advection.

Key Words: Indian monsoon; onset; deep convection; cumulonimbus; cumulus congestus; dry intrusion; land–atmosphere interaction; water cycle

Received 21 September 2015; Revised 30 March 2016; Accepted 5 April 2016; Published online in Wiley Online Library

1. Introduction

The Indian monsoon affects the lives of more than a billion people in South Asia and supplies around 80% of the annual rainfall total between June and September. The largely agricultural society is highly dependent on monsoon rains and is very sensitive to any variation in their timing, intensity and duration. This is particularly true of the monsoon onset, since its timing in relation to the sowing of crops is crucial for their survival. Despite its importance, currently there is no accepted physical explanation for the advance of the monsoon onset across India. This article offers a conceptual model for this phenomenon.

The traditional India Meteorological Department (IMD) definition of the monsoon onset relates to the first sustained

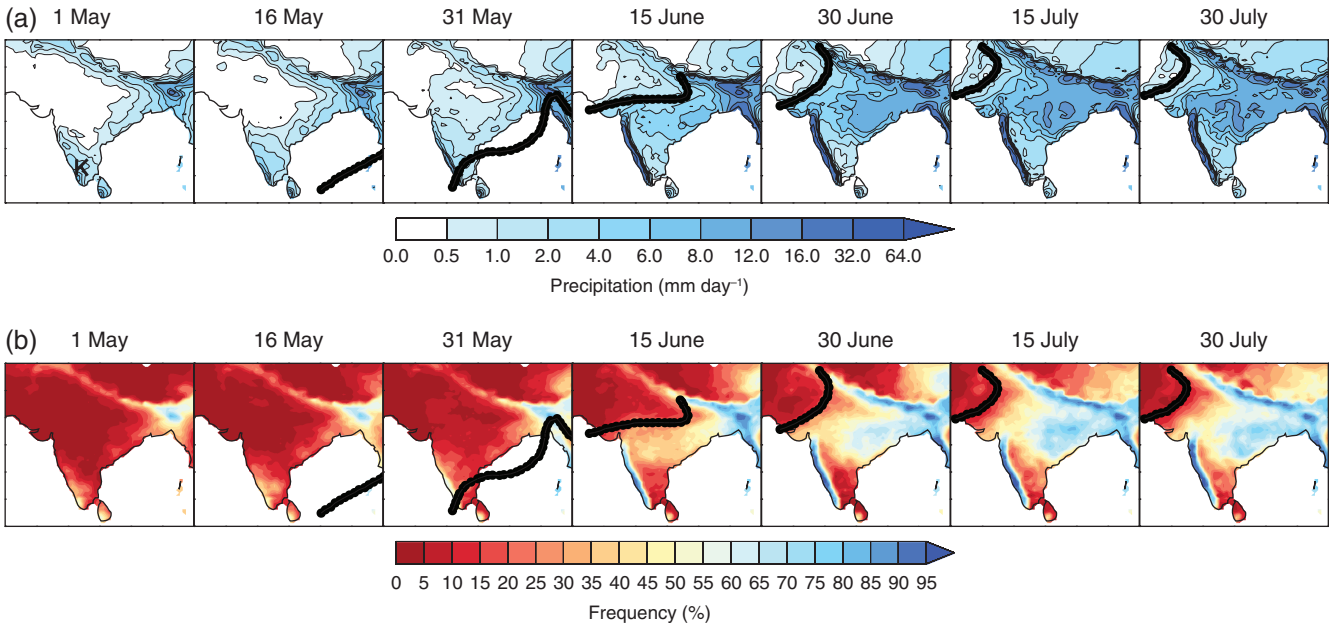

Figure 1. Statistics of rainfall over India during the monsoon onset from the APHRODITE 0.5° gridded gauge-based dataset, averaged over 1951–2007, with each panel labelled with the middle day of its 5-day period. Climatological isochrones of monsoon progression as defined by the IMD are also shown by the thick black lines; the closest in time in each panel (the five chosen isochrones being 25 May, 1 June, 15 June, 1 July and 15 July). (a) Mean rainfall (mm day^{-1}) and (b) mean frequency of rainfall occurrence, expressed as a percentage. The IMD standard rainy day threshold of 2.5 mm is used to define rainfall occurrence. The state of Kerala is indicated in (a) with a letter 'K'.

rains over Kerala in southwest India, climatologically occurring on 1 June with a standard deviation of 8–9 days (Ju and Slingo, 1995; Krishnamurthy and Shukla, 2000). Moron and Robertson (2014) have conducted an updated analysis of monsoon onset at the local scale, based on 1° gridded rainfall data from 1901 to 2004, demonstrating typical deviations in the median onset date of 10–20 days over large parts of northern India. Variations in the onset have large impacts on society, and recent years have provided large contrasts. The rapid advancement of the monsoon onset in 2013, reaching the north by mid-June, led to considerable flooding in Uttarakhand state. In contrast, the delayed onset in 2014 led to extended heatwave conditions in northern India.

On the regional scale, the annual advance of the monsoon onset has been well defined on the basis of long-term measurements. Charts compiled by the IMD demonstrate a northwest advance of the onset isochrone (or the northern limit of the monsoon) across India from 1 June, reaching the border with Pakistan around mid-July. A consequence is that the rainy season in northwest India is considerably shorter than in the south. Figure 1 shows the relationship between the IMD-defined climatological mean northern limit of the monsoon and statistics of the rainfall as observed by gauges over the continent, for three key pentads covering the overall onset period. Figure 1 confirms that the IMD northern limit isochrones are an effective climatological measure of the monsoon onset. To the south of the northern limit, rainfall is both heavier and more frequent; however, to the north of the northern limit, intermittent rainfall does occur, albeit with much lower frequency.

Despite the importance of the monsoon and its onset, monsoon simulation remains a challenge to the modelling community, for reasons which are not well understood, and therefore better physical understanding of the monsoon onset is still needed. Atmosphere-only and coupled general-circulation models (GCMs) typically suffer dry biases over much of the Indian peninsula and have shown little improvement as models have developed from the Coupled Model Intercomparison Project CMIP3 to the CMIP5 era (Sperber *et al.*, 2013). CMIP5 coupled GCMs feature rainfall onset dates around 10 days too late over much of India, with poorly defined progression across the country (Sperber *et al.*, 2013). Atmosphere-only models often exhibit dry biases over the Indian peninsula and wet biases over the equatorial Indian Ocean. Coupled models exhibit corresponding cold sea-surface temperature (SST) biases in this region through a negative feedback with the rainfall biases, enhancing moisture transport towards India (Levine *et al.*, 2013). However, coupled model cold biases introduced in Arabian Sea SST during spring restrict the moisture available to the subsequent monsoon season (Levine and Turner, 2012; Levine *et al.*, 2013) and the same models feature systematically delayed monsoon onsets (Levine *et al.*, 2013). Model cold biases in the Arabian Sea are caused by anomalous advection of cold, dry air over that region from the northwest in winter and spring (Marathayil *et al.*, 2013), with the suggestion that these biases are themselves caused by the upper-level westerly jet that is situated too far south at this time of year (Sandeep and Ajayamohan, 2014), perhaps related to slow development of the Tibetan High, and cold continental surface temperatures in winter (Levine *et al.*, 2013).

On the continental scale, some mechanisms have been proposed, to explain the timing of monsoon onset; however, these mechanisms generally do not explain the spatial structure of the onset and the progression from south to northwest. The onset of the monsoon is associated with the intensification of vertically integrated moisture flux in the westerly flow from the Arabian Sea, and the development of the monsoon trough lying across northern India, which supports the Arabian Sea inflow as well as establishing southeasterly moisture flux into the Indo-Gangetic plain from the Bay of Bengal (e.g. Raju *et al.*, 2005 and references therein). In association with these changes, the subtropical westerly jet shifts from a position over India to a latitude north of the Himalayas, consistent with anticyclonic circulation in the upper troposphere. These changes in circulation are associated with the reversal of the meridional tropospheric temperature gradient (Li and Yanai, 1996), with strong warming of the air over the Tibetan Plateau in spring, and therefore an easterly thermal wind, consistent with the monsoon westerlies and upper-tropospheric easterlies over India. Subsequent analysis over an extended period in European Centre for Medium-range Weather Forecasts (ECMWF) ERA-40 reanalysis data has confirmed the relationship between the reversal of the meridional tropospheric temperature gradient and the monsoon onset over Kerala (Xavier *et al.*, 2007). Such dynamical controls on the onset have been related to the causes of early and late onset. For instance, Joseph and Srinivasan (1999) related the occurrence of wet and dry years to large-amplitude stationary Rossby wave trains just before the monsoon onset, showing a barotropic structure in the subtropical jet. Furthermore, Xavier *et al.* (2007)

diagnosed a significant relationship between the vertical circulation and the monsoon onset timing: enhanced subsidence over the Indian region is associated with weaker vertical mixing and a delayed onset. Chakraborty *et al.* (2006) showed that the onset of the monsoon occurred only after surface moist static energy crossed a threshold value, and vertical velocity became upward.

A number of studies have discussed the role of both thermal and mechanical forcing by the Tibetan Plateau and the Himalayan region on the onset patterns of both the South Asian and East Asian monsoons (e.g. Wu and Zhang, 1998; Wu *et al.*, 2007, 2012a; Boos and Kuang, 2010; Liu *et al.*, 2014) and the role of air–sea interaction (Wu *et al.*, 2012b), indicating that the complex and unique orography of the region and the particular arrangement of the land and ocean are inherent in the development of the large-scale circulations that drive the pattern of monsoon onset.

In addition to the seasonal perspective on monsoon onset, Indian monsoon depressions also play a role in the onset, both regionally and locally, imposing important synoptic variability on the process. For instance, in 2014 a low-pressure pattern over the northern Bay of Bengal restricted monsoon activity to eastern areas of India, after which westward movement of a low-pressure area in the period 11–16 July facilitated the onset of the monsoon in the northwest of the country (Pai and Bhan, 2014). Other processes on subseasonal time-scales, such as the Madden–Julian Oscillation, also influence the monsoon onset (Wheeler and Hendon, 2004; Pai *et al.*, 2011).

Although a self-consistent explanation for the establishment of the summer monsoon state exists, understanding of the basic monsoon dynamics fails to account for the progression of the rains from the extreme south to the extreme northwest of India, a distance of approximately 2000 km, over a 6-week period. Inspection of the analysed wind fields in the lower and mid-troposphere (Figure 2) in conjunction with the rainfall evolution (Figure 1) shows that the monsoon onset, in terms of the advance of the northern limit of the rains, cannot be explained simply in terms of the advection of moisture into the continent by the time-mean low-level flow. The low-level flow does strengthen around this time, but the monsoon onset generally moves from the south toward the northwest of the continent, perpendicular to (to the left of) the monsoon winds at 850 hPa, which are predominantly westerly at this level. The monsoon moves upwind relative to mid-level winds, at 600 hPa (Figure 2(a)–(c)). For instance, around 23°N 82°E on 15 June, the mean position of the northern limit of the monsoon is moving quite rapidly *toward* the northwest, while the winds are still *from* the northwest at both 850 and 600 hPa, and the 600 hPa winds are flowing through and to the south of the northern limit. In the ERA-Interim data, vertically integrated moisture flux (Figure 2(m)–(o)) confirms the conclusion that the movement of the northern limit of the monsoon does not follow the advection of moisture, and cannot easily be explained by the field of moisture flux convergence in this model.

The observation that the movement of the monsoon onset toward the northwest cannot be explained by moisture advection in the same direction raises general questions about the dynamics and thermodynamics of onset progression, and challenges our understanding of the basic balances controlling the mean monsoon. Krishnamurti *et al.* (2012) have shown that the movement of the onset isochrone is associated with a progressive wetting of the land surface, a few hundred kilometres to the north of the isochrone, encouraging deep convection to occur just to the north of the isochrone, and hence the northward progression of the northern limit of rains. It was suggested that this wetting of the soil to the north of the onset isochrone is due to precipitating anvils of deep convection forming within the rainy areas to the south, and advected north and northwest by the upper-tropospheric winds.

In addition to considering the role of the low-level monsoon winds in the variability of Indian rainfall, various authors have recognised the importance of mid-level dry air, descending in northwesterly flow from over the Indus valley and Thar Desert region. Sawyer (1947) discussed the vertical structure and slope of the 'Inter-tropical front' (ITF, which might be associated with the northern limit of the monsoon rain) during the later part of the monsoon, based on the analysis of radiosondes and meteorological flights made in the period 23 August to 1 September 1945. Sawyer's paper showed that in the extreme northwest of India, at this time of year, a mid-tropospheric dry layer overlies the moist monsoon layer, intruding toward the southeast. This structure appeals to the 'air-mass thinking' that prevailed in midlatitude synoptic meteorology at that time, and the basic structure was first proposed by Ramanathan and Banerjee (1931), in the study of pre-monsoon storms in the Bay of Bengal. Ramanathan and Banerjee (1931) emphasised the importance of low stability (dry) air in the location and intensity of the storms, the air moving from the land to over the Bay in northwesterly winds around 3 km altitude. The heaviest rain and most violent squalls were consistently associated with the leading edge of a northwesterly flow of over-running dry unstable air. Houze *et al.* (2007) and Romatschke and Houze (2010) also relate this structure to convective type and organisation, showing how the dry, near-adiabatic layer lying above the monsoonal air gives rise to intense and organised mesoscale convective systems (MCSs). Similar thermodynamic profiles are observed in other monsoonal regions around the world (e.g. West Africa: Parker *et al.*, 2005) and over the Great Plains of the USA, and are commonly associated with MCS development.

On longer time-scales, Bhat (2006) showed that the dry monsoon year of 2002 was caused by very dry northwesterly winds capping the monsoon inflow over the Arabian Sea, notably in July of that year. The local response of the monsoon system was itself linked to large-scale drivers, the passage of the Madden–Julian Oscillation leading to rapid development of El Niño (Saith and Slingo, 2006). More generally, Krishnamurti *et al.* (2010) then showed how dry spells in the monsoon are associated with incursions of mid-level dry air, in the form of West Asian desert air incursions, linked to a blocking high (diagnosed in the 700–300 hPa levels) over the Arabian Peninsula, and to a northward shift of rainfall over West Africa. Sabin *et al.* (2013) showed the importance of mid-level dry air intrusions in model differences in the representation of the monsoon rainfall, and the model representation of monsoon depressions.

The aim of this article is to explain the basic processes controlling the dynamics and thermodynamics of onset, and to explore the role of the interaction between mid-level dry air and cumulus convection in the onset process. It is argued that the onset process is dependent on a weakening of the mid-level dry northwesterly intrusion. Section 2 presents the datasets used in the analysis. Sections 3 and 4 present kinematic and thermodynamic perspectives on the onset, followed by discussion and conclusions in section 5.

2. Data

In this article we attempt to analyse the dynamics and thermodynamics of monsoon onset using, as far as possible, observational data in preference to model data. This is because models are known to have substantial biases in their representation of rainfall over the Indian subcontinent, and are known to have significant limitations in their representation of convective clouds in particular.

Radiosonde data have been obtained from the Integrated Global Radiosonde Archive (IGRA) and mean profiles have been computed for the years 1971–2014, for the stations marked in Figure 3. The data have been interpolated in the vertical using simple linear interpolation, before averaging over all profiles. Launches at 0000 and 1200 UTC have been combined in the averaging. For key dates the soundings have been averaged over 5-day pentads; the numbers of soundings used at each station in the pentads is a minimum of 225 and a maximum of 406 for the Indian stations; at Kandahar the total is a minimum of 72 soundings for the 1 June pentad. For computational of deep convective properties, the lifted parcel is based on the

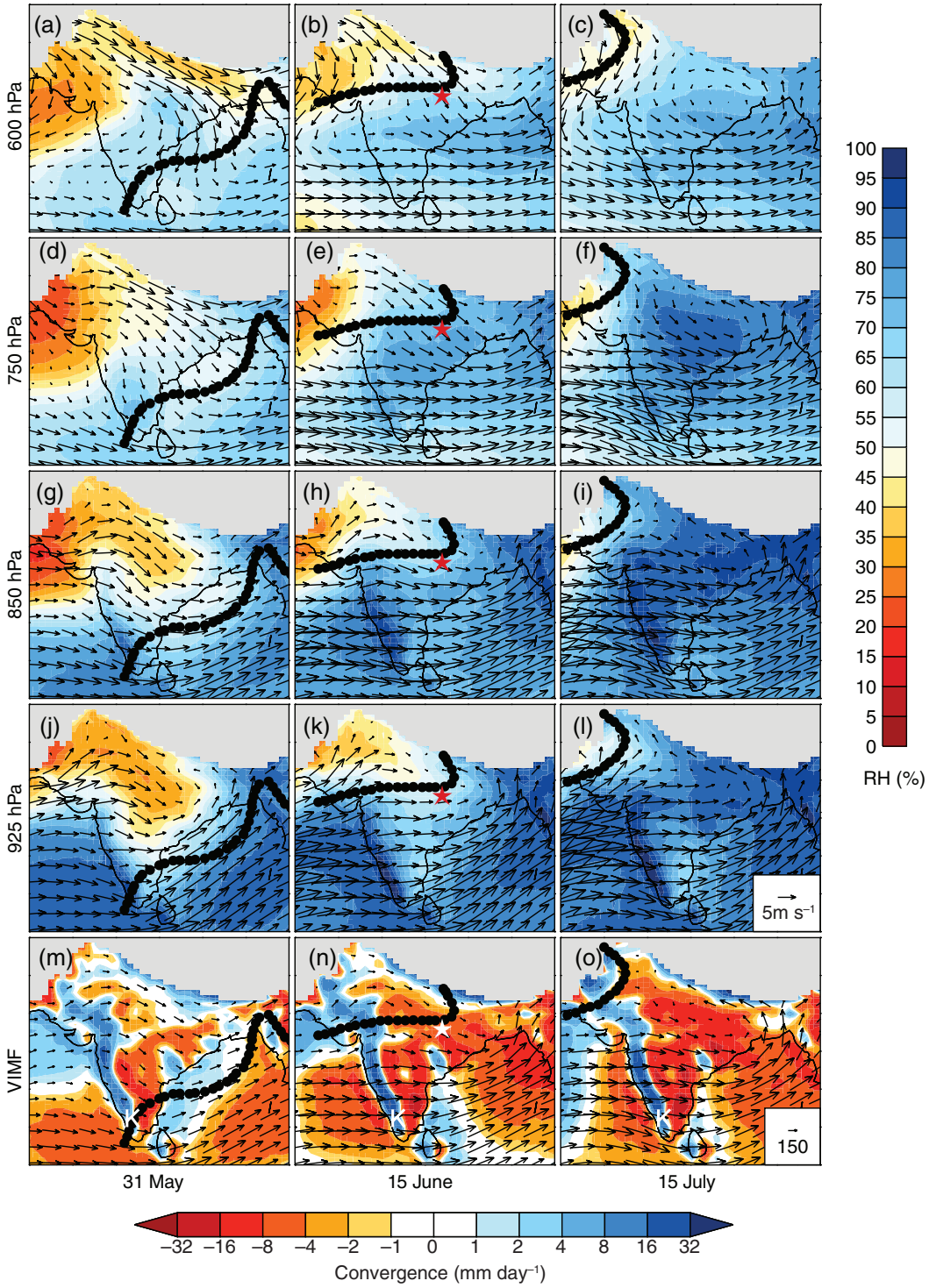

Figure 2. Mean relative humidity (shading, %) and horizontal winds (vectors, m s^{-1}) from ERA-Interim reanalysis averaged over 5-day periods centred on (a,d,g,j,m) 31 May (around first onset; left), (b,e,h,k,n) 15 June (mid-onset; centre) and (c,f,i,l,o) 15 July (full monsoon; right column), over the years 1979–2014. The fields are shown on levels (a–c) 600 hPa (top row), (d–f) 750, (g–i) 850 and (j–l) 925 hPa. The lower row (m–o) shows vertically-integrated moisture flux (VMF) vectors (kg m^{-1} s^{-1}; integration is performed from the surface to 100 hPa) and moisture flux convergence, scaled to represent mm day^{-1} of equivalent rainfall. Monsoon progression isochrones are also shown as in Figure 1. The location 23°N 82°E mentioned in the text is indicated with a star, and the state of Kerala with a letter 'K'. Regions in which the orographic height exceeds 1000 m are shaded in grey.

mean thermodynamic properties of the layer 50–500 m above the surface. The daily analysis of soundings at Nagpur was computed for the period 1991–2015, for which we have the local onset dates (Nandankar *et al.*, 2011), and between 17 and 33 soundings were averaged for each day.

Synoptic station data were obtained from the Met Office Integrated Data Archive System (MIDAS) at the British Atmospheric Data Centre (BADC), for the period 1980–2013. In analysing the SYNOP low cloud type (C_L) observations, these data have been classified into four categories, representing (i) zero low cloud, or very shallow cloud leading to little vertical moisture change ($C_L = 0$ or 1), (ii) low cloud which penetrates in the vertical and causes some moisture exchange, but without cumulonimbus forming ($C_L = 2$, 4 or 8), (iii) cumulonimbus ($C_L = 3$ or 9), and (iv) other low cloud, stratocumulus and stratus ($C_L = 5$, 6 or 7).

The monsoon northern limit isochrones were taken from the climatological mean lines issued by the IMD and digitised using cursor graphical input software. Representative dates are used in the subsequent analysis to represent conditions of key phases of the onset process: 15 May for pre-onset; 31 May or 1 June immediately before or after the first onset; 15 June for mid-onset; and 15 July, around the end of the monsoon onset period. Years of early and late onset at Nagpur (Nandankar *et al.*, 2011) have

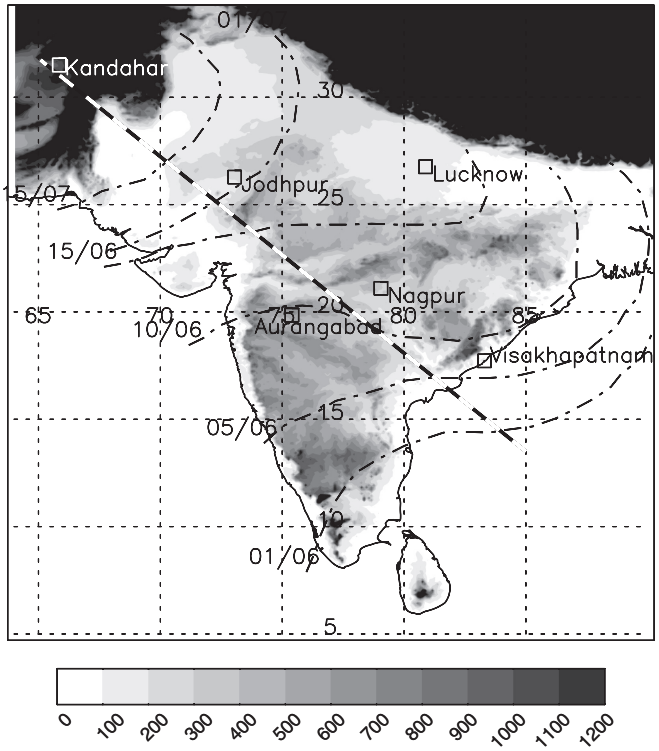

Figure 3. Map of the study region, with topographic height contoured in metre. Locations of radiosonde stations used in the analysis are labelled, as well as the line (dashed) used as the axis for the creation of vertical cross-sections from the radiosonde data (Figure 7). Monsoon progression isochrones (day/month) are also shown, as in Figure 1.

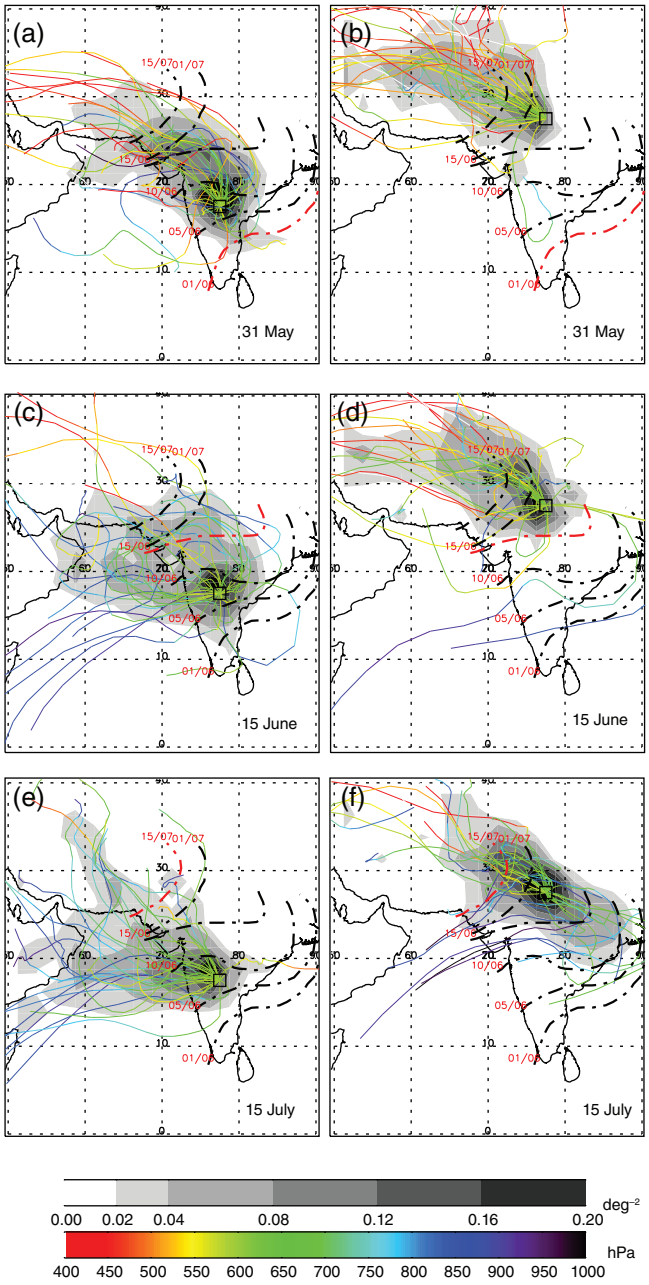

Figure 4. Six-day back-trajectories showing the characteristics of the mid-level northwesterly inflow to India, for the period 1981–2013, from the ECMWF operational model and ERA-15. For each year, five back-trajectories have been launched, initialised with 0.5° spacing centred on the point marked with a square. Grey shading indicates the density of 6 hourly back-trajectory points per one-degree square, normalised by the total number of trajectories (165). The central trajectory is also plotted for each year of the sample, and coloured according to its pressure. Central termination points are at 600 hPa, at 0000 UTC on (a,b) 31 May, (c,d) 15 June and (e,f) 15 July located at (a,c,e) 77.5°E, 17.5°N and (b,d,f) 77.5°E, 27.5°N. Climatological isochrones of monsoon progression as defined by the IMD are also shown by the thick black lines, the closest to the time of each panel marked in red.

been selected if the onset occurred 3 or more days from 15 June, from which the years (1992, 1995, 1997, 2002, 2003, 2005, 2006, 2007, 2009, 2011, 2012, 2014) were taken to be late, and (1991, 1994, 2000, 2001, 2008, 2013) to be early. Although the use of a single location to identify early and late onset years may not be more widely representative, it has the advantage of being an objective measure.

Rainfall data have been taken from the APHRODITE 0.5° gridded rain-gauge dataset for monsoon Asia (Yatagai *et al.*, 2012), consisting of daily gauge data inputs over the 1951–2007 period for much of monsoon Asia. This dataset has been shown to perform well in comparison to IMD's own rain-gauge products for India (Prakash *et al.*, 2015). The OLR dataset is a gridded satellite-derived product with temporal interpolation (Liebmann and Smith, 1996).

All model data plotted are from the ERA-Interim reanalysis (Dee *et al.*, 2011), for the 36 years 1979–2014. However, trajectories have been computed using the Web Trajectory Service from the British Atmospheric Data Centre (BADC), which uses the ECMWF archive of ERA-15 and operational ECMWF products.

A daily climatology of surface soil water saturation index is computed using observations from the Advanced Scatterometer (ASCAT) on board the MetOp-A satellite (Bartalis *et al.*, 2007) for the years 2007–2012. These observations are made typically once per day and are gridded at 0.25° × 0.25°.

3. Kinematics of onset

As indicated in Figure 2, the mean winds from reanalysis fields at different dates show upstream, or at least cross-stream movement of the northern limit relative to the low and mid-level flow. Around the time of first rains in the extreme south of India (around 1 June), the 850 hPa westerly flow has strengthened relative to the pre-monsoon period, with maximum intensity in the south (Figure 2(g)). At 600 and 750 hPa there is a significant northwesterly flow extending from Afghanistan right across the subcontinent, down to the southeast coast of India: in subsequent analysis it will be seen that the 600 hPa level is at the heart of an intrusion of mid-tropospheric dry air. As the northern limit of the monsoon progresses toward the northwest over the next 14 days, the 600 hPa northwesterly flow also withdraws; it remains strong in the far northwest, but to the south of the northern limit the 600 hPa winds back to a more westerly direction, associated with the monsoon trough lying just to the south of the northern limit at this level.

Figure 2 shows climatological mean flow and therefore does not provide information on eddy transport of moisture, for instance by synoptic systems. In order to have confidence in interpreting the dynamics and kinematics of the system, we need to consider synoptic time-scales and the trajectories of individual air parcels. Therefore Figures 4 and 5 explore some details of the

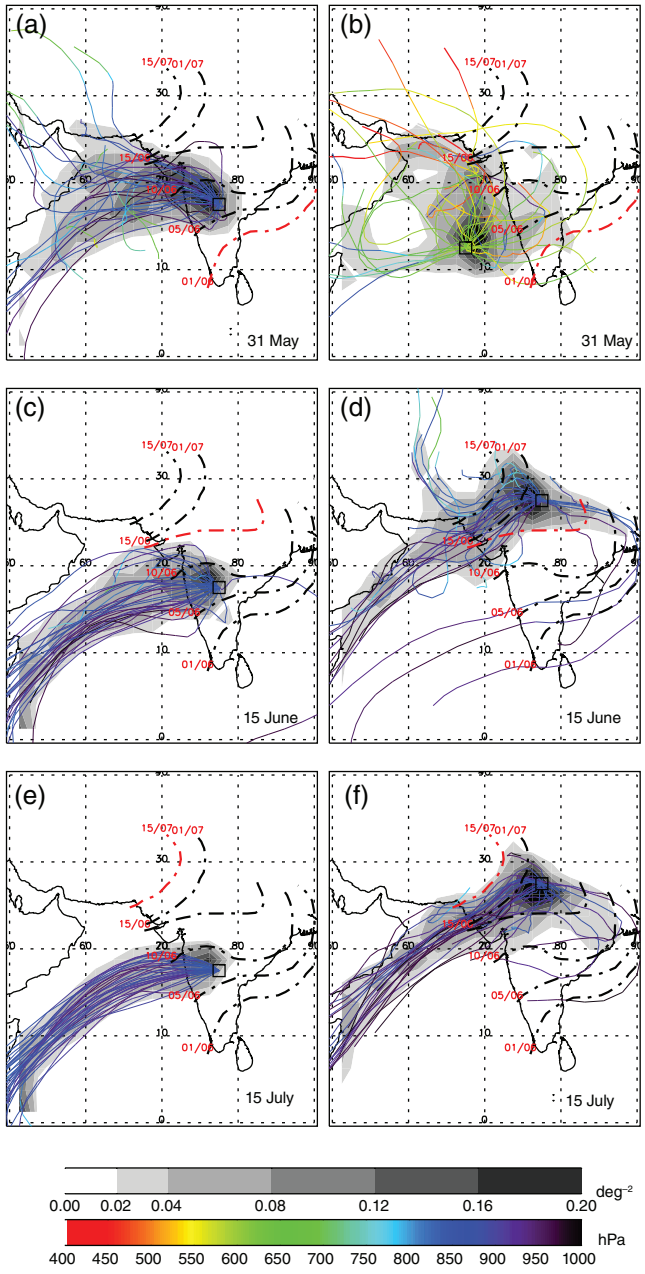

Figure 5. Six-day back-trajectories, computed as in Figure 4. Termination points are at 0000 UTC on (a,b) 31 May, (c,d) 15 June and (e,f) 15 July, at a level of 850 hPa, except for panel (b), which terminates at 600 hPa, with a new location, over the Arabian Sea.

onset process in terms of the trajectories of air arriving over India around the time of monsoon onset (in the region of the northern limit of rains).

Immediately before the climatological mean time of first onset in the south, 31 May, both trajectory end-points (at 600 hPa) in Figure 4(a) and (b) lie to the north of the northern limit, and trajectories terminating at these locations in most years have originated as descending air from the northwest. These trajectories are consistent with the examples of Ramanathan and Banerjee (1931) for several case-studies from 1929. Figure 2, and subsequent analysis, confirms this air to be very dry and characterised by a profile of low static stability. In contrast, the low-level air arriving at 850 hPa on 31 May (Figure 5(a)) is flowing mostly from the west, from low levels over the Arabian Sea, and in the south of India this pattern is maintained throughout the onset period (Figure 5(c) and (e)).

After the passage of the northern limit, the 600 hPa trajectories tend to back, and more commonly ascend from the west. The change in 600 hPa wind direction is associated with the general cyclonic circulation found to the south of the northern limit as the monsoon trough strengthens. Again, the pattern of wind to the south of the northern limit is consistent with Ramanathan and Banerjee's (1931) case-studies. By 15 June, the northern limit has moved beyond (to the north of) the terminus-point of the trajectories shown in Figures 4(c) and 5(c). Since this point is now to the south of the northern limit, many of the trajectories terminating at 600 hPa arrive from lower levels over the Arabian Sea, although some still contain air which has descended from the northwest. In contrast, in Figure 4(d) the trajectories remain north of the northern limit of the monsoon, and almost all trajectories arriving here at 600 hPa descend from the northwest.

By 15 July, both end-points are to the south of the northern limit. In the south (Figure 4(e)), air at 600 hPa most frequently consists of trajectories rising from the southwest, but in the north (Figure 4(f)) there is a split in the trajectory origins, with air parcels in some years arriving at 600 hPa in descending air from the northwest, and in other years as flow from the southeast, recurving around the monsoon trough. These southeasterly trajectories are sometimes bringing mid-level air from the Bay of Bengal, probably associated with synoptic enhancement of the monsoon trough, for instance by monsoon depressions, and the air is likely to be moist. Similarly, the air arriving at 850 hPa over northern India (Figure 5(f)), while most commonly originating in the southwest monsoon flow from the Arabian Sea, in some years represents recurving flow from the Bay of Bengal.

The trajectories confirm Bhat's (2006) observation that mid-level dry air is also an influence over the monsoon inflow over the Arabian Sea. Immediately before the onset (Figure 5(b)) many trajectories arriving at 600 hPa over the Arabian Sea represent dry air from the northwestern desert regions. During later stages of the onset (not shown), the descending air is less common in this region, but the lack of ascent in the trajectories, combined with their origins over arid land areas, suggests that they often represent dry intrusions over the monsoon layer.

It is worth remarking more generally on the trajectories originating over the Bay of Bengal in these results. Some 600 hPa parcels originate from over the Bay of Bengal (Figure 4(f)). This source region is much less common for trajectories ending at the 850 hPa level (Figure 5(f)). It is only when considering end-points very close to the Himalayas (not shown), that a significant fraction of the 850 hPa trajectories originate in the east.

We can consider the time-scale of air parcel motion relative to the rate of advance of the northern limit of the monsoon. From the trajectory plots of Figures 4 and 5, it appears that advection time for air moving across the subcontinent is a few days (these figures show 6-day trajectories). The advection time of the mid-level and planetary boundary-layer air is therefore short relative to the much slower advance of the monsoon rains (∼30–45 days, in the opposite direction to the mid-level flow). Therefore, on a daily time-scale, air is streaming through the system faster than the system itself is evolving, and the northern limit of the monsoon is in some kind of slow evolution relative to advection of the air.

Ramanathan and Banerjee (1931) and Sawyer (1947) presented the ITF (which we may associate with the northern limit of monsoon rain) as an air-mass boundary: in contrast, Figures 2, 4 and 5 indicate that the northern limit is a transition zone in a much more dynamic flow, with air always moving relatively rapidly through this zone. The progression of the northern limit of the monsoon does not correspond to the advection of a material 'front', but instead corresponds to the temporal evolution of a very active transition zone. The northern limit can be regarded as a zone in which there is a balance between fast processes of horizontal advection and cloud vertical mixing, and in which the time-scales of airflow, on the order of days, are faster than the time-scales of the system evolution.

4. Thermodynamics of the onset

Figure 6 shows mean vertical profiles from three stations along a section from the northwest to southeast of India (radiosonde

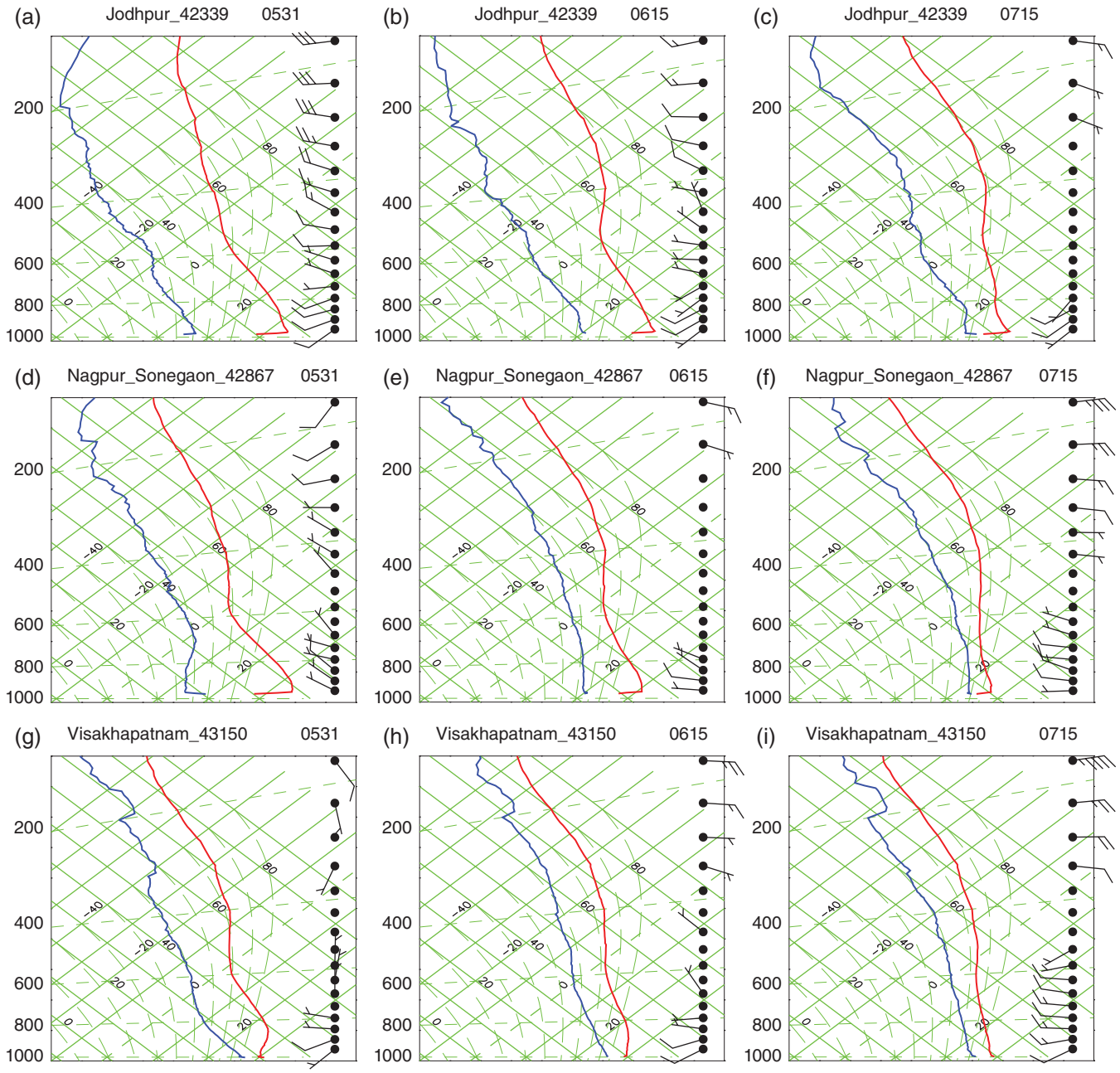

Figure 6. Climatological mean radiosonde profiles from (top row; a–c) Jodhpur, (d–f) Nagpur and (g–i) Visakhapatnam, representing a transect from the northwest to southeast of India. Temperature (red) and dew point (blue) profiles are plotted as tephigrams, for 31 May (around first onset; panels (a,d,g)), 15 June (transition period; (b,e,h)) and 15 July (around the end of onset; (c,f,i)). Note that a nocturnal stable layer is often seen close to the surface in these plots, due to the high numbers of 0000 UTC soundings in those cases.

station locations are marked in Figure 3), at key dates in the onset period. Mean profiles are shown as the onset progresses, and allow us to consider the implications of these changes for moist convection.

Just before the onset, on 31 May (Figure 6(a)) the mean profile at Jodhpur in the northwest is characterised by a deep, dry well-mixed layer (600–800 hPa), with northwesterly or westerly winds that are descending from the high topography to the north and west. Beneath this layer the profile is more stable, with a southerly component to the winds. This structure persists throughout the onset period (Figure 6(b)) in this location.

At Nagpur (Figure 6(d)) and Visakhapatnam (Figure 6(g)), the dry mid-level air is also evident on 31 May, but becoming shallower in the vertical toward the southeast. At low levels at Visakhapatnam the profile is more nearly pseudoadiabatic, characteristic of shallow cumulus and congestus. The 'elevated mixed layer' in the profile observed at Visakhapatnam (Figure 6(g)) has been observed in many other parts of the world and is described generally by Carlson (1998, chapter 16) and for West Africa by Parker *et al.* (2005). The presence of this elevated mixed layer is characteristic of high convective available potential energy (CAPE) and high convective inhibition (CIN), leading to shallow cumulus clouds, as well as the likelihood of intense cumulonimbus storms.

At all times and locations, the higher levels (above 600 hPa) are nearly pseudoadiabatic, as is commonly observed in the Tropics (e.g. Betts, 1986). The Visakhapatnam profile (Figure 6(g)) therefore makes a transition with height that may be described as pseudoadiabatic at low levels, adiabatic in the 600–800 hPa layer, and back to pseudoadiabatic above this.

At all locations, the subsequent progression of the monsoon onset is associated with falling low-level temperatures, increasing relative and absolute humidity, and lowering lifting condensation level (consistent with Figure 2). As time progresses, the dry mid-level layer is also moistened and evolves from a nearly adiabatic profile toward a pseudoadiabatic profile, for example in the 600–800 hPa layer at Nagpur, Figure 6(d)–(f). The transition with time of this layer from dry adiabatic to moist adiabatic involves cooling at the low levels, as well as warming in the mid-levels. The 31 May profile at Visakhapatnam

(Figure 6(g)) has very similar characteristics to Nagpur on 15 June (Figure 6(e)) and by the time the monsoon has reached the far northwest (Jodhpur on 15 July; Figure 6(c)) the northwestern profile is also consistent, with an elevated mixed layer separating low-level and upper-level profiles that are more nearly pseudoadiabatic.

At all three stations, the wind profiles show consistent evolution over time. Westerly wind components on 31 May at higher levels (above 700 hPa) gradually reduce over time, to be replaced by upper-level easterly winds associated with the upper-level anticyclone known as the Tibetan or South Asia High. However, at lower levels the westerlies continue, and a northerly component continues to be present around 700 hPa at Nagpur (Figure 6(f)) and Visakhapatnam (Figure 6(i)).

To synthesise these radiosonde data, and include data from additional stations, Figure 7 shows a collection of vertical sections from the northwest to the southeast of the region, crossing the northern limit of the monsoon, and presented at different dates during the onset period. In Figure 7(a), the monsoon layer is seen as a wedge of high water-vapour mixing ratio, deeper to the southeast and becoming shallower toward the northwest. As the monsoon progresses into 15 June (Figure 7(b)), the monsoon layer deepens, although the horizontal gradient does not fully disappear, with the column moisture being lower in Jodhpur than in the sites to the southeast of this. The slope of the leading edge of the humid layer appears to get steeper as the monsoon progresses, with more uniform depth to the monsoon layer southeast of Aurangabad by 15 July (Figure 7(c)).

The relationship of the mixing ratio with the wind field (in Figure 7(a)–(c)) can be used to infer the moisture flux characteristics (as mapped in Figure 2(m)–(o)). As the monsoon progresses, the low-level westerly mean flow becomes deeper, while the relatively dry mid-level flow originating from the northwest becomes meridionally narrower and much less deep, confined to no lower than 600 hPa. Comparing Figure 2(m) with (n) shows a dramatic increase in the vertically integrated moisture coming from the west all along the west coast, which in Figure 7(a) and (b) is represented by a deeper layer of high mixing ratio, and a stronger component of the wind vector normal to this vertical section.

The relative humidity (RH) field (Figure 7(d)–(f)) exerts a significant control on the occurrence of deep convection, through its suppression, by dry entrainment, of the first cumulus clouds. Therefore, in the northwest, we expect that cumulus clouds are limited in their vertical extent (confirmed in subsequent analysis of synoptic station data). In turn, the detrainment of moisture from cumulus clouds increases the RH of the ambient air as the dry layer moves toward the southeast, causing the layer of high RH to deepen toward the southeast. The signature of detraining cumulus congestus clouds can be inferred from the mid-level wedge of high relative humidity around $T = 0\,^{\circ}\mathrm{C}$, or approximately 550 hPa (this is a preferred level for detrainment from congestus: Johnson *et al.*, 1996). This high RH may also be due to partial detrainment from deep cumulonimbus storms at remote locations. The mid-level humid layer is manifest in a tendency for the occurrence of altocumulus clouds, which may have a very strong impact on the surface energy balance; at least comparable to, if not greater than the influence of aerosol (as indicated, in the African environment, by Marsham *et al.* (2013)). Around 15 June (Figure 7(e)), the monsoon layer of high low-level RH has a significant slope downwards toward the northwest, similar to but not exactly following the slopes in water vapour mixing ratio and θ_e.

The mid-level dry air descending from the northwest is seen as an intrusion of air of low equivalent potential temperature (θ_e) from May onwards, with the dry intrusion first extending right down to the southeast coast (Figure 7(g), and as seen at 800 hPa at Visakhapatnam in Figure 6(g)). Subsequently, the mid-level dry intrusion can be seen to retreat toward the northwest (Figure 7(h)–(i)). The lowest θ_e values are found around 500–600 hPa, around or slightly below the freezing level, despite the RH being slightly higher in this layer. At low levels the layer of high θ_e is deeper to the southeast but its slope is not identical to that of water vapour mixing ratio. As the onset proceeds, θ_e increases to the southeast and increases in time everywhere, notably at low levels.

The saturated equivalent potential temperature field (θ_{es}) is useful in indicating the moist convective regimes (Figure 7(j)–(l)): when θ_{es} is constant with height the profile is pseudoadiabatic and consistent with moist adjustment by convective clouds. Around the time of onset (Figure 7(j)), a near-pseudoadiabatic profile is seen in all of the Indian profiles, both at low levels where shallow cumulus may be active, and at higher levels from about 600 to 400 hPa. At these stations there is a strong gradient of θ_{es} with height in the 800–600 hPa layer, below the freezing level, and associated with low dry static stability in the northwesterly dry intrusion.

At a given pressure level, θ_{es} is homomorphic with temperature, so the cooling of the low levels over the continent is apparent in θ_{es} as time progresses, beginning in the interior and progressing to the northwest and southeast of this observational section with time. This cooling is presumably related to a combination of processes: strengthening cool advection from the west; convective downdraughts; increased cloud cover; and increasing soil moisture and vegetation cover reducing the surface sensible heat flux. The cooling is accompanied by higher RH and θ_e. At mid-levels, the θ_{es} field shows the change in the large-scale temperature gradient, with cooler air over the deserts of the northwest gradually warming through the onset period.

By 15 June (Figure 7(k)), the vertical profile of θ_{es} has become more nearly constant with height in the southeast, indicating a profile that is close to pseudoadiabatic and controlled by frequent deep convective clouds. Toward the northwest, a cooler mid-level layer remains, around 400–500 hPa, which corresponds to a cold point in the profile and is probably linked to the global tropical cold-point in temperature at $T = 0\,^{\circ}\mathrm{C}$ (Betts, 1986). The cool layer of low θ_{es} represents the upper part of a mid-level intrusion of dry air of low (dry) static stability; the strong gradient of θ_{es} around 600–700 hPa in the northwest is associated with near-constant potential temperature. Above this, the profile is more stable than the pseudoadiabat, and represents a barrier to deep cloud formation. Many cumulus congestus clouds will detrain at this layer, although some have sufficient buoyancy and kinetic energy to penetrate through to higher altitudes and develop into deep cumulonimbus.

The changes in θ_e and θ_{es} shown in Figure 7(g)–(l) can be related to the changes in stability conditions for convective clouds, and specifically, rain-bearing cumulonimbus. In particular, the transition of the mid-level layer of low static stability (around 800–600 hPa) toward a pseudoadiabatic profile later in the season is associated with a warming of the profile above 600 hPa (Figure 7(j)–(l)) and a cooling of the profile below this. The higher-level warming tends to reduce CAPE, while the lower-level cooling acts to reduce CIN. However, during the same period, the low-level θ_e is increasing (Figure 7(g)–(i)), which tends to reduce CIN and increase CAPE. In combination, CIN is being reduced by both the lower tropospheric cooling and the boundary layer θ_e increase, but the effects of these layers on CAPE act in opposition, with the mid-level temperatures tending to reduce CAPE and the boundary layer θ_e tending to increase it. As noted above, these CAPE and CIN changes are accompanied by a general increase in the relative humidity of the lower troposphere (Figure 7(d)–(f)), which permits the increasing development of convective clouds generally.

The spatial separation of the radiosonde stations used in Figure 7 precludes a very fine-scale analysis of the structure of the northern limit. More detail, and a consideration of earlier and later periods in the onset, can be inferred from inspection of the time series of profiles at one station, Nagpur, as shown in Figure 8 (note that we also repeated this analysis for Lucknow and obtained consistent results).

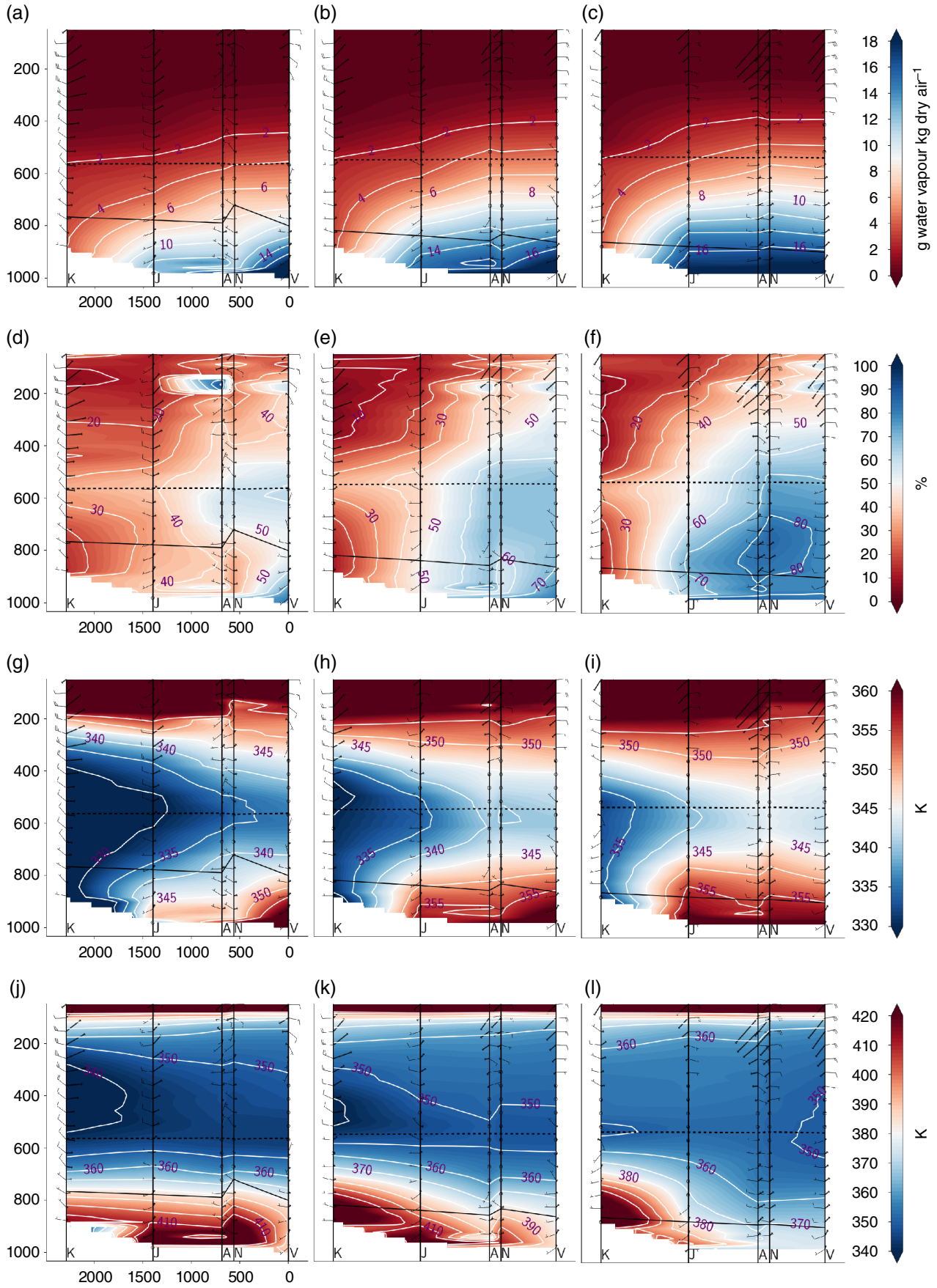

Figure 7. Northwest to southeast sections of atmospheric thermodynamics and winds from radiosonde data in the period 1971–2014, on (panels a,d,g,j) 1 June, (b,e,h,k) 15 June and (c,f,i,l) 15 July. Vertical lines show the locations of the radiosonde stations, labelled as 'V' = Visakhapatnam, 'N' = Nagpur, 'A' = Aurangabad, 'J' = Jodhpur and 'K' = Kandahar (station locations are marked on Figure 3). The panels show (a–c) water vapour mixing ratio (g kg^{-1}), (d–f) relative humidity (%), (g–i) θ_e (K), and (j–l) θ_{es} (K). On each panel the winds are shown in two forms: wind vanes and feathers indicate the horizontal winds relative to geographical coordinates, while the vectors show the horizontal winds relative to the vertical section shown on Figure 3, with a horizontal vector representing flow parallel to the section. The solid line marks the LCL and the dotted line marks the $T = 0\,^{\circ}$C level.

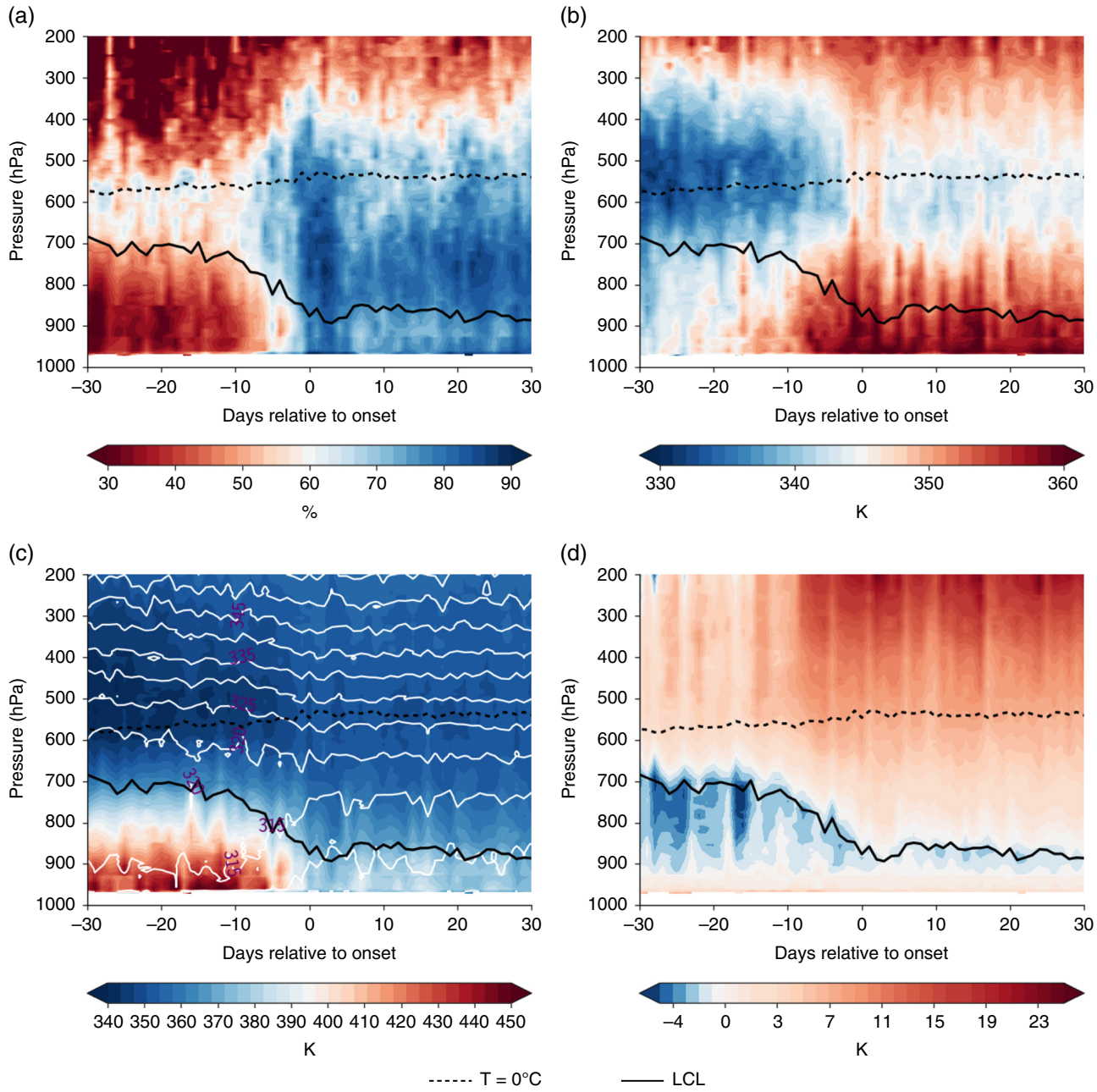

Figure 8. Time–pressure sections for Nagpur showing (a) RH (%), (b) θ_e (K), (c) θ_{es} (K) with virtual potential temperature θ_v overplotted (contours, K) and (d) buoyancy of lifted boundary-layer parcels (K). All panels show LCL (solid line) and level of $T = 0\,^{\circ}$C (dotted line). The profiles are computed for days relative to the onset date at this station on each year (Day 0 in the time axis) for the period 1991–2015: over this period, the mean arrival of the northern limit at this station is 16 June.

The field of RH (Figure 8(a)) shows how a pre-monsoon maximum of cloud in the altocumulus layer around $T = 0\,^{\circ}$C (around 600–550 hPa, at the top of the elevated mixed layer) is replaced, on the arrival of the monsoon, by a much deeper layer of high RH, with a peak at the top of the boundary layer, around 800–750 hPa. Importantly, the mid-level layer of high RH which follows the $T = 0\,^{\circ}$C line in the pre-monsoon season becomes much deeper from about 12 days before the onset date, as the lifting condensation level (LCL) descends, and as the upper limit of the layer of high RH also extends upwards above $T = 0\,^{\circ}$C. This pattern is consistent with a prevalence of cumulus and congestus clouds in the pre-monsoon season capped around the $T = 0\,^{\circ}$C level, and increasing penetration of these clouds into the higher tropospheric levels in the days before onset. These changes are strongly suggestive of the action of cumulus clouds in moistening the tropospheric profile over time.

The very dry layer above the LCL (around 45–60% in the pre-onset period), which tends to suppress early cumulus development, increases its RH in the 5 days before onset to 60–75% or greater, in the mean. Similarly, Figure 8(b) shows increasing low-level θ_e as well as increasing θ_e in the mid-level dry intrusion, in the 20 or 30 days preceding onset, with relatively high values above the LCL from about 8 days before onset. Although θ_e at low levels is increasing from 20 to 30 days prior to onset, it is only from around 10 days before onset that evidence of significant deeper penetration of convection above the $T = 0\,^{\circ}$C level is observed (Figure 8(a)). Figure 8(b) also demonstrates the value of this daily time series relative to the more coarse temporal and spatial resolution of Figure 7, in showing that there is a maximum in θ_e at mid-levels of the profile, in approximately the 5 days surrounding the local onset.

The field of θ_{es} (Figure 8(c)) confirms and extends the thermodynamic structure seen in the tephigrams of Figure 6. At the beginning of this period, Nagpur shows a deep adiabatic layer at low levels, characterised by the wide spacing of the 315 and 320 K virtual potential temperature contours. From around 10 days prior to onset, these contours begin to move closer together, reflecting a transition towards a pseudoadiabatic profile (θ_{es} more nearly constant with height toward the end of the onset period). Although there is a warming of the mid-level air (above

600 hPa) throughout the 30 days before onset, the increasing dry static stability around the onset is dominated by the cooling of the air at low levels below 700 hPa in the 10 days preceding onset, as seen in Figures 7(j)–(l) and 8(c). At the same time, from Figure 8(b) it is apparent that the low-level air, while cooling, is also increasing its θ_e. The plot of parcel buoyancy (Figure 8(d)) reflects the combination of these changes. Around 10 days prior to the onset, the LCL is descending, as low-level air becomes more humid. In this period the CIN layer becomes shallower over time, due to higher boundary-layer θ_e, and therefore lower LCL, but also due to cooling of the air below 700 hPa. From about 8 days prior to onset, when the low-level θ_e becomes large, parcel buoyancy increases substantially, and there is much higher positive buoyancy in mid- and upper-tropospheric levels (e.g. 200–400 hPa in Figure 8(d)), despite the mid-level warming of the profile in this period.

The time–pressure plots of Figure 8 may be complemented by the time series of rainfall and soil moisture relative to the onset isochrones plotted by Krishnamurti *et al.* (2012; their Fig. 9), which show rainfall increasing around 1000 km north of the northern limit, and soil moisture following this, increasing significantly from 150 to 500 km ahead of the northern limit. The increasing soil moisture, and developing vegetation, reduce the Bowen ratio, which in turn contributes to increased θ_e in the boundary layer through a reduction in dry entrainment (Betts and Ball, 1995). These soil moisture feedbacks may be responsible for the significant increase in θ_e seen around 10 days before onset in Figure 8(b), and collocated with the time at which there is evidence of convective cloud-tops developing higher than the $T = 0\,^{\circ}\mathrm{C}$ level (at which point, we assume that precipitating convection is increasingly likely).

In conclusion, the set of plots presented in Figures 7 and 8 confirm that the onset of the monsoon is characterised by the moistening of a midlevel wedge of dry air, lying in the levels around 400–700 hPa, emanating from the northwest. Figure 8(a) is indicative of the moistening being caused, at least in part, by increasing cumulus activity over time. The dryness of the mid-level air suppresses moist convection, as does the relatively high CIN in the pre-monsoon period. The first monsoon rains occur in the extreme south because this is the furthest extension of the mid-level dry intrusion, and the first position on the section at which CIN is low enough, and the mid-levels sufficiently humid, to support active clouds. From the high buoyancy in Figure 8(d), we infer that CAPE also reaches maximum values around the time of local monsoon onset (possibly a few days before), but this effect is not enhanced directly by the withdrawal of the mid-level northwesterly dry intrusion, because this withdrawal corresponds to a slight warming of the mid-levels. Instead, the increasing CAPE is caused by increasing boundary-layer θ_e. At the same time, around local onset, CIN is a minimum, due to high parcel θ_e and to cool air around and above the LCL.

Since the winds have a component from the northwest in the dry layer, the retreat of the mid-level dry layer toward the northwest must be caused by a net moistening, itself due to a changing balance between the dry advection and moistening by convection from below. This increase in moistening can be brought about by several external processes, all of which are observed:

- a strengthening of the low-level southwesterly monsoon moisture flux, leading to more active clouds (Figures 2(m)–(o) and 8(a)), or
- increased soil moisture and evaporation into the boundary layer leading to more active clouds (Krishnamurti *et al.* (2012) and Figure 8(a)), or
- a weakening of the dry mid-level northwesterly winds (Figures 2, 4–6, and 7(a)–(c)),

or, most likely, a combination of these processes. In addition, there are some 'internal' processes which contribute to the increased moistening of the mid-levels, notably the reduction of CIN (Figure 8(d)) by lower-tropospheric cooling, which may itself be caused by convective cloud adjustment. Although these influences cannot easily be separated in the observational analysis, some intriguing evidence comes from modelling results. Bollasina and Ming (2013) found that monsoon onset still proceeded in idealised GCM simulations of the monsoon system in which the global conditions (sea-surface temperatures and solar radiation) were set to a 'perpetual May', implying that the physics of the onset is controlled by 'internal' processes of adjustment and evolution to the May-time global forcing, rather than being driven by external dynamical factors. In particular, in the model, soil moisture increases ahead of the precipitation front, consistent with the observations of Krishnamurti *et al.* (2012). Further evidence comes from the idealised studies of Choudhury and Krishnan (2011), who showed how the mid-level circulation is very sensitive to the convective and stratiform fractions within MCS events in the monsoon region. An internal feedback between the thermodynamic and wind profiles which dictate the convective events, and the circulation over the subcontinent, appears to be occurring. More recently, Liu *et al.* (2014) discussed the 'monsoon onset barrier' which, in May, prevents the maximum in monsoon precipitation progressing from the Bay of Bengal over the Indian subcontinent. Liu *et al.* (2014) argued that the monsoon onset barrier involves a dynamical response to the convective heating over the Bay of Bengal at this time, causing westerly shear and subsidence over the subcontinent; we can see that this pattern enhances the mid-level dry advection seen in pre-onset profiles over India (e.g. Figure 6(g)).

More deeply untangling the various contributions of differential advection, vertical moisture transport by clouds, soil moisture and surface fluxes is not trivial, since they are all interlinked. However, it is informative to inspect the evolution of the cloud and soil moisture fields across the northern limit of the rains. Figure 9 presents the mean low-cloud reports from Indian synoptic stations, in relation to the monsoon northern limit and the mean soil moisture map.

Around 31 May, clear skies and very shallow cumulus clouds (Figure 9(a)) are common in the northwest and north because the boundary layer is dry, and there is dry air overlying the boundary layer to suppress any cumulus by dry entrainment. Deep cumulonimbus clouds (Figure 9(c)) are observed in the south and east of India, even though most of India lies to the north of the northern limit on this date. Soil moisture (indicated by surface water saturation index in Figure 9) has begun to increase at some locations ahead of (north of) the northern limit, notably on the Western Ghats and along the east coast of India; in these regions the field of surface water saturation index shows values less than 0.2 at the beginning of May (not shown). Active non-precipitating cumulus (which includes cumulus congestus; Figure 9(b)) occurs most commonly in the transition between these 'clear' and 'cumulonimbus' zones, and is moistening the relatively dry mid-levels in this region (e.g. Figure 7(b), (e), (h)). Taking the panels of Figure 9(a)–(c) together, we can infer a gradual transition in the low-cloud field, from the northwest to the south, of clear and shallow cumulus, developing into more common occurrence of deeper cumulus and congestus which moisten the dry mid-levels, and most frequent cumulonimbus in the south and east.

Around 15 June, the soils across much of central India have moistened, stimulating vegetation growth and a transition from fluxes dominated by sensible to latent heat. At the same time it can be seen that the occurrence of 'clear' conditions (Figure 10(a)) is less frequent as the monsoon has advanced, and these conditions of weak vertical moisture transport have effectively retreated into the far northwest. As may be expected with the arrival of monsoon rains, occurrence of cumulonimbus has increased, especially in locations to the south and east of the northern limit (Figure 10(c)). Intermediate cumulus (Figure 10(b)) has been maintained almost everywhere as the monsoon has arrived, but has somewhat decreased in locations to the south of the

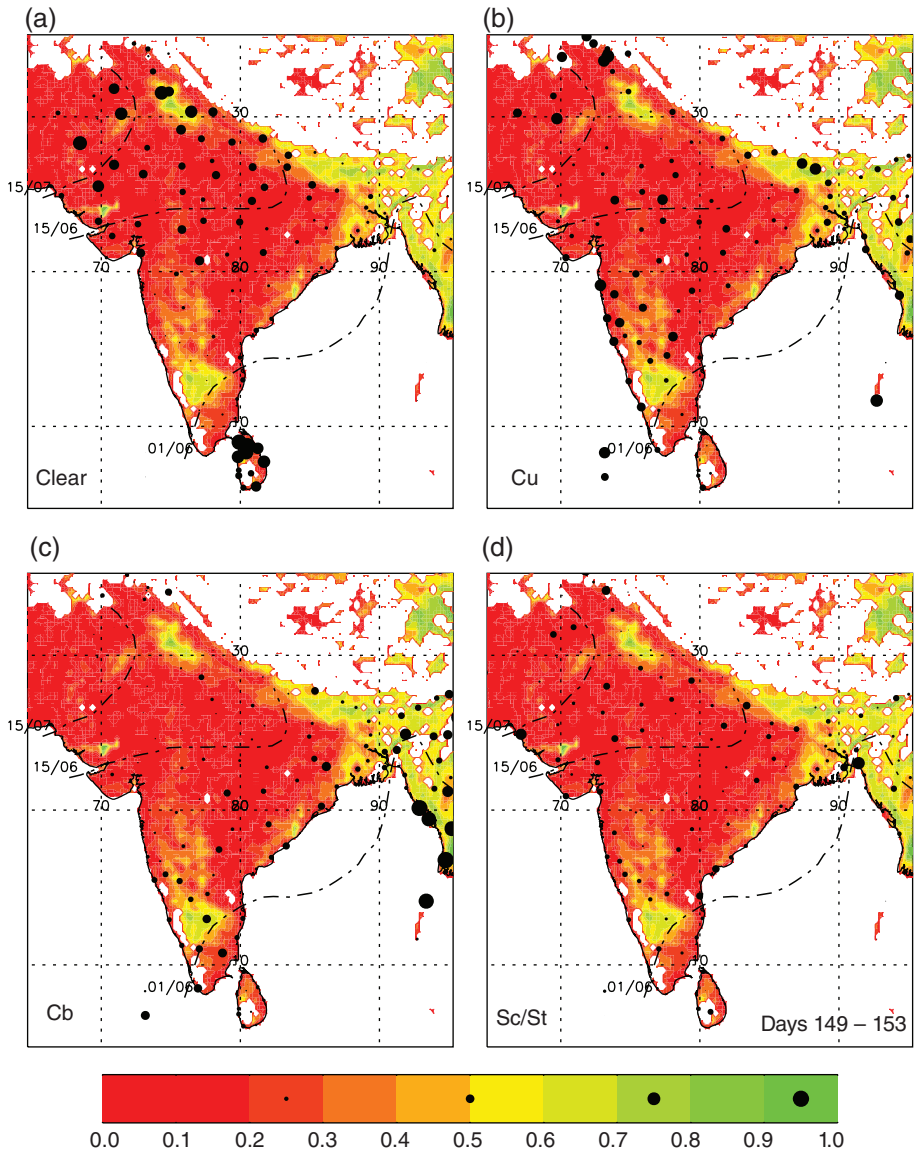

Figure 9. Climatological maps of surface water saturation index for the years 2007–2012 (shaded; repeated in all panels) and low-cloud fractions (filled circles) for 1200 UTC, each as a 5-day mean centred on 31 May. Low-cloud data are taken from synoptic station reports and represent (a) zero low cloud, or shallow cumulus; (b) deeper cumulus and cumulus congestus; (c) cumulonimbus; and (d) stratocumulus or stratus. The diameter of the filled circle represents the fraction of low cloud reports that occupy the given category at that station, with examples superposed on the colour bar at the appropriate fraction. For more details of the cloud classifications, see section 2. Selected isochrones of the monsoon onset are shown as in Figure 1.

northern limit, and apparently increased to the north (notably at stations where the occurrence of clear skies is becoming less frequent). Stratus and stratocumulus clouds (Figure 10(d)) have increased in frequency in the west and east of India. Overall, comparison of Figures 9 and 10 shows a northwestward shift of the transition zone between shallow cumulus in the northwest and deep convection in the southeast.

The aggregated effect of the cloud fields leads to a remarkably smooth transition in mean outgoing long-wave radiation (OLR) over the continent. Figure 11 shows the mean OLR for three key dates in the onset period. The transition in space from high temperatures, with very low cloud cover in the northwest, and cold temperatures in the deep convective regions south of the northern limit, is dramatic. The relatively smooth gradient in OLR from northwest to southeast combines the effects of shallower clouds in the northwest, and less frequent clouds there also (Figures 1 and 10). For instance, this OLR gradient in Figure 11(b) corresponds to the slope in height of the high RH zone around 15 June in Figure 7(b) and gives a three-dimensional perspective to the role of the mid-level dry intrusion in controlling cloud cover over India at this period. Romatschke and Houze (2010) have shown how the deepest convection in the monsoon period is influenced by the mid-level humidity, with deep convective cores in the pre-monsoon season found in the extreme east of India, transitioning to the northwest in the full monsoon. In both seasons, the deepest convection tends to occur where there are strong surface humidity gradients and a dry layer aloft; these conditions are met in the vicinity of, and usually to the north of the northern limit of the monsoon. Indeed, Ramanathan and Banerjee (1931) found the most intense Bay of Bengal storms at the southeastern limit of the mid-level intrusion of dry air from the land. Furthermore, Krishnamurti *et al.* (2012) argued that it is the dynamics of the local storms around the northern limit of the monsoon, whose anvils may propagate north of that limit and wet the soil in the pre-monsoon region, which control the progression of onset. For these reasons, it is desirable to obtain better understanding, through improved *in situ* observations, of the atmospheric structure in the vicinity of the northern limit of the monsoon as it moves northwards; this dynamical structure is related to the occurrence of severe weather, as well as being related to the advancement of the monsoon over land.

5. Discussion

During the monsoon onset over India, the mid-levels are characterised by an intrusion of dry mid-to-low troposphere air in northwesterly winds, as the air descends from Afghanistan

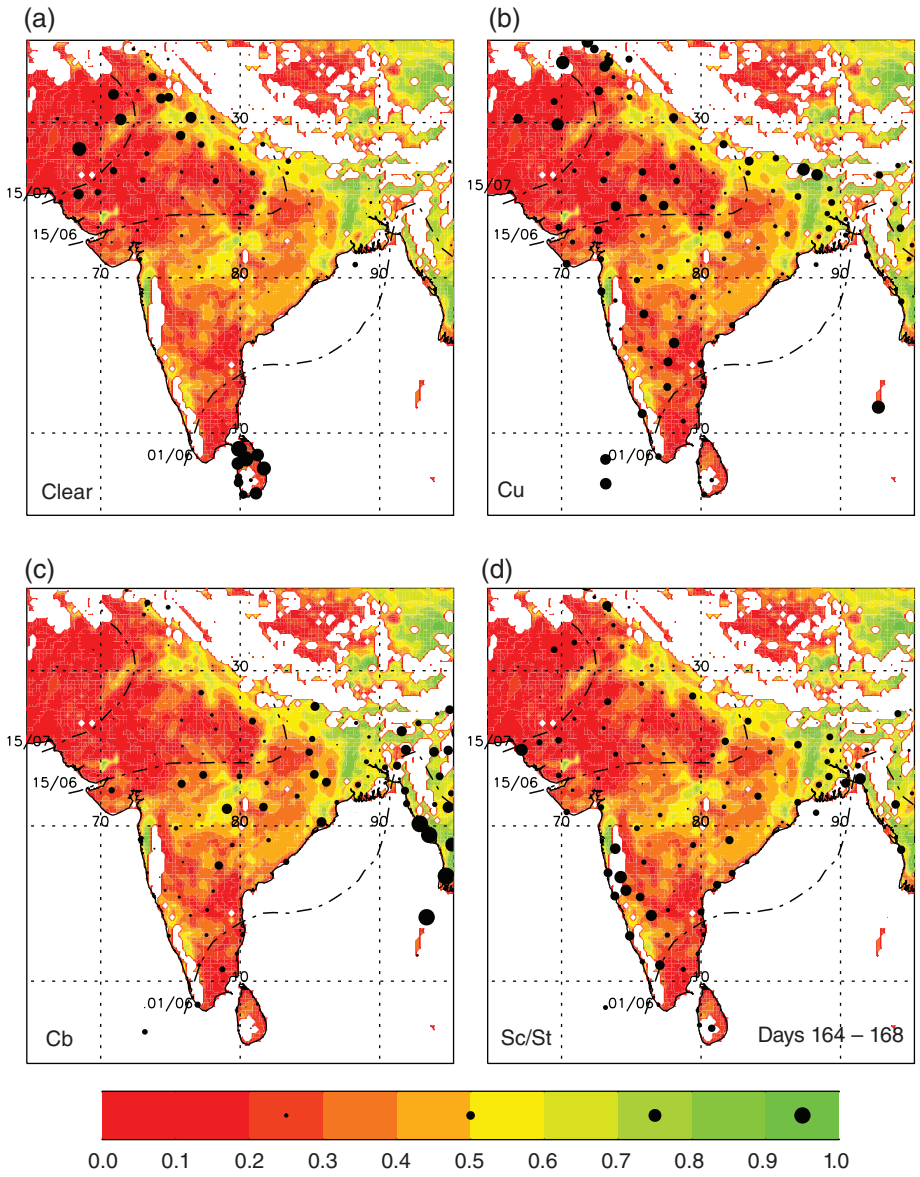

Figure 10. As Figure 9, but for 15 June. Low-cloud data are taken from synoptic station reports and represent (a) zero low cloud, or shallow cumulus; (b) deeper cumulus and cumulus congestus; (c) cumulonimbus; and (d) stratocumulus or stratus.

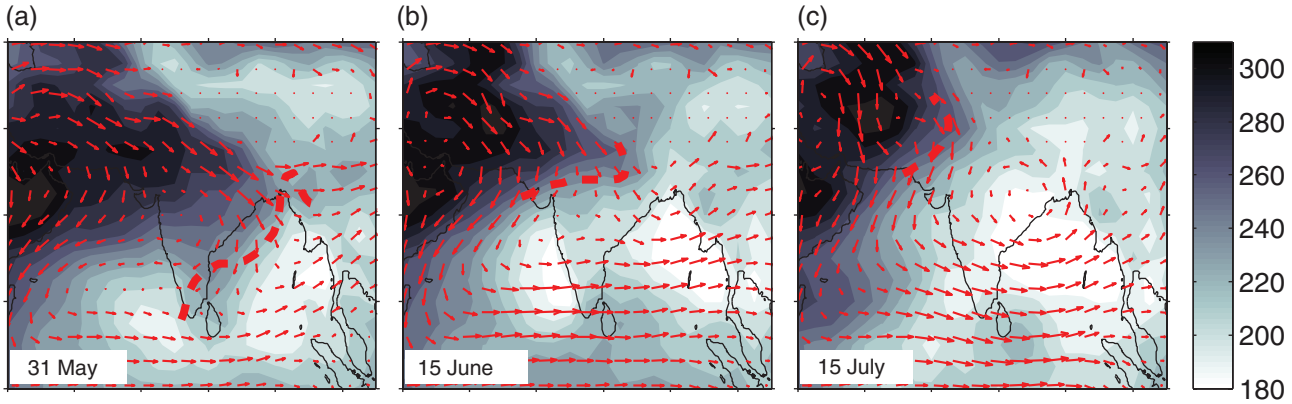

Figure 11. Mean observed outgoing long-wave radiation (shading, W m^{-2}) and ERA-Interim 600 hPa winds (vectors), averaged over multiple years for the dates 13–18 June. The OLR data are averaged over the years 1974–2013 and the winds over the years 1979–2013. The dashed red line marks the average northern limit of the monsoon on 15 June, as defined by the IMD.

and Pakistan down over India. In the pre-monsoon period this very dry layer suppresses rainfall, even in late May when the monsoon winds have begun. However, the moisture supply in the monsoon winds supports the development of shallow cumulus and congestus convection, as well as some occasional precipitation from cumulonimbus (Figures 1 and 9), which build progressively as the mid-level flow moves from the northwest. We can see this progression in the infrared imagery, with the mean cloud-top temperature decreasing steadily from northwest to southeast.

As noted by Bhat (2006), results from the TOGA-COARE experiment demonstrate a similar preconditioning of the column by shallow cumulus and congestus, but in a temporal sense rather

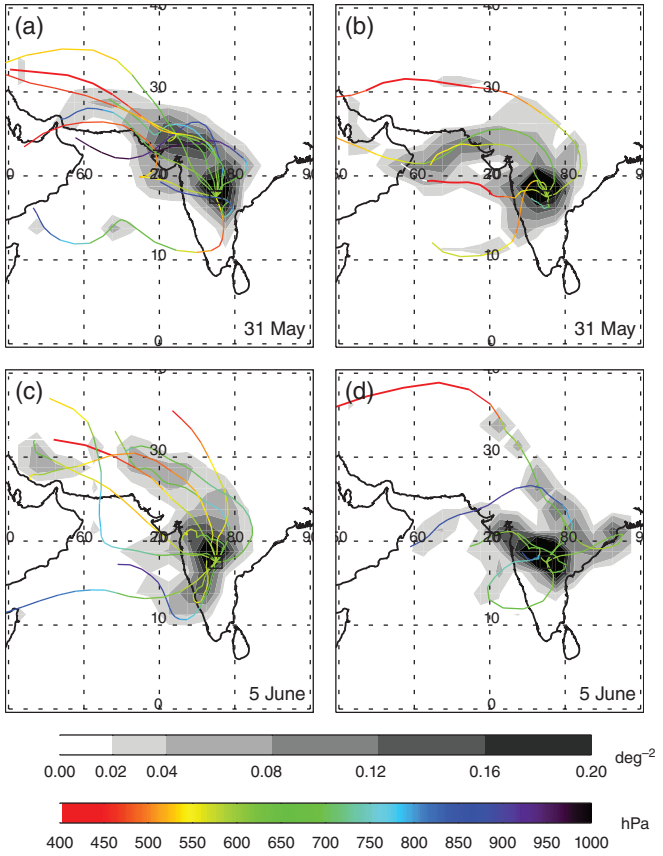

Figure 12. Six-day back-trajectories, computed as in Figure 4, for years of (a,c) late onset and (b,d) early onset at Nagpur. Termination points are at 0000 UTC on (a,b) 31 May, (c,d) 5 June at a level of 600 hPa.

than a Lagrangian sense (Mapes and Zuidema, 1996; Parsons *et al.*, 2000). In TOGA-COARE, dry intrusion events were followed by a period of several (10–20) days of suppressed rainfall during which the mid-level dry intrusion was progressively humidified by shallow cumulus and congestus. Over India we infer this process occurring in a Lagrangian sense, as the mid-level dry air moves from the northwest. The dry air is moistened from below as it moves toward the southeast, and the profile most conducive to deep convective rainfall is therefore in the southeast. This process is no doubt enhanced at the monsoon onset by coastal and orographic triggering in the west.

As the season and the onset develop, the northern limit progresses towards the northwest because the thermodynamic balance between mid-level dry advection and cloud vertical transports that determines the northern limit position is altered: the rate of moistening of the dry layer increases, relative to the horizontal advection of the dry air.

- As the monsoon layer gets deeper, the southwest monsoon winds occupy a deeper layer, and therefore there is deeper cumulus and the rate of moistening of the dry layer increases;
- the northwest winds at 600 hPa are weakened and back (whether due to local mixing effects, local effects of the cloud heating on pressure gradients, or large-scale pressure gradient changes);
- there is storage of moisture in the soil, which reduces the Bowen ratio, and maintains a cool, moist and shallow boundary layer of high θ_e.

Each of these processes has the potential to be enhanced by transient and synoptic events. For instance, isolated convective rainfall events ahead of the northern limit wet the soil, and therefore encourage subsequent cloud formation and moistening of the dry layer aloft (and downwind). On a larger scale, synoptic events such as monsoon depressions may temporarily retard the mid-level dry advection, and allow rainfall to occur and soil moisture to increase. Alternatively, large-scale changes in the mid-level circulation, perhaps related to western disturbances (Dimri *et al.*, 2015), may allow the dry intrusion to strengthen during the monsoon season, and suppress rainfall until the dry air is moistened by cumulus.

Krishnamurti *et al.* (2012) argued that precipitating anvils moving northwards from the vicinity of the onset isochrone cause the northward movement of that isochrone. Here we suggest that it is more generally the change in thermodynamic balance to the north of the isochrones which causes the propagation; wetting of the surface by pre-monsoon rain is one element in this changed balance, but really it is the changing thermodynamic profile for deep convection which matters, and this is more generally controlled by low-level moist advection, mid-level dry advection and instability, as well as the soil moisture which feeds the boundary layer.

The land surface state has an important role to play in the maintenance and variability of rainfall. Although on a daily time-scale the pre-monsoon precipitation does not increase the column moisture (in fact it decreases column moisture of the atmosphere), the fact that air is flowing through the system faster than the monsoon progression means that each rainfall event is storing moisture in the continental surface to be released into the boundary layer by surface fluxes on later days. Once rainfall has happened in a particular location, this wets the surface and some water will be recycled. Tuinenburg *et al.* (2012) estimated water vapour recycling over the continent and found that in the pre-monsoon months (March to May) there is increasing retention of evaporated water within India, rising to around 50–60% in the Ganges Basin in June. The recycling of moisture in this way increases the total (atmospheric plus surface) column water over the continent, makes the planetary boundary layer (PBL) over wet surfaces cooler and more humid, with higher θ_e than over drier surfaces elsewhere, and increases the chance of rain on subsequent days. Through the onset period, the vegetation cover is also developing rapidly. The access to water at greater depths in the soil provided by the roots allows evapotranspiration to be maintained during dry spells of a few days.

Identifying the importance of mid-level dry air in the monsoon onset (and in monsoon breaks: Krishnamurti *et al.*, 2010) raises the possibility that demarking contrasts in mid-level dryness will be a useful operational weather forecasting tool. Indeed, Ramanathan and Banerjee (1931) were already associating the location of the most intense, squally storms with the leading edge of a mid-level dry layer. More recently, forecasters in West Africa are now plotting mid-level dry air boundaries on their synoptic charts, to indicate areas of suppressed convection and areas where mid-level dryness may enhance squalls (Fink *et al.*, 2011). Forecasters for tropical regions often prefer to use the 500 hPa level to evaluate the levels of humidity which may encourage or suppress convection (J. F. R. Galvin, 2015; personal communication; see also Galvin, 2009). More careful analysis of the controls on convection over the Indian region is needed, but Figures 7 and 8, consistent with the results of Ramanathan and Banerjee (1931), suggest that the 600–700 hPa levels may be better for the identification of mid-level humidity boundaries over India.

In emphasising the role of the mid-level dry intrusion, it is important to consider the thermodynamic origins of this air. The intrusion is characterised by subsidence (Figure 4), which causes the relative humidity to fall. The trajectories pass over the dry desert regions in the northwest of India and Pakistan, where dry convection leads to a cool profile up to around the freezing level (e.g. Figure 6(a)). Although the dry adiabatic mixing over the desert leads to surprisingly high relative humidity, and intermittent altocumulus clouds, in the cool air at around 600 hPa (Figure 6(d)–(f)), mixing ratio remains low, because the latent heat fluxes over the desert are very low (Figure 6(a)–(c)). Dynamically, the heat-low which develops over the desert regions

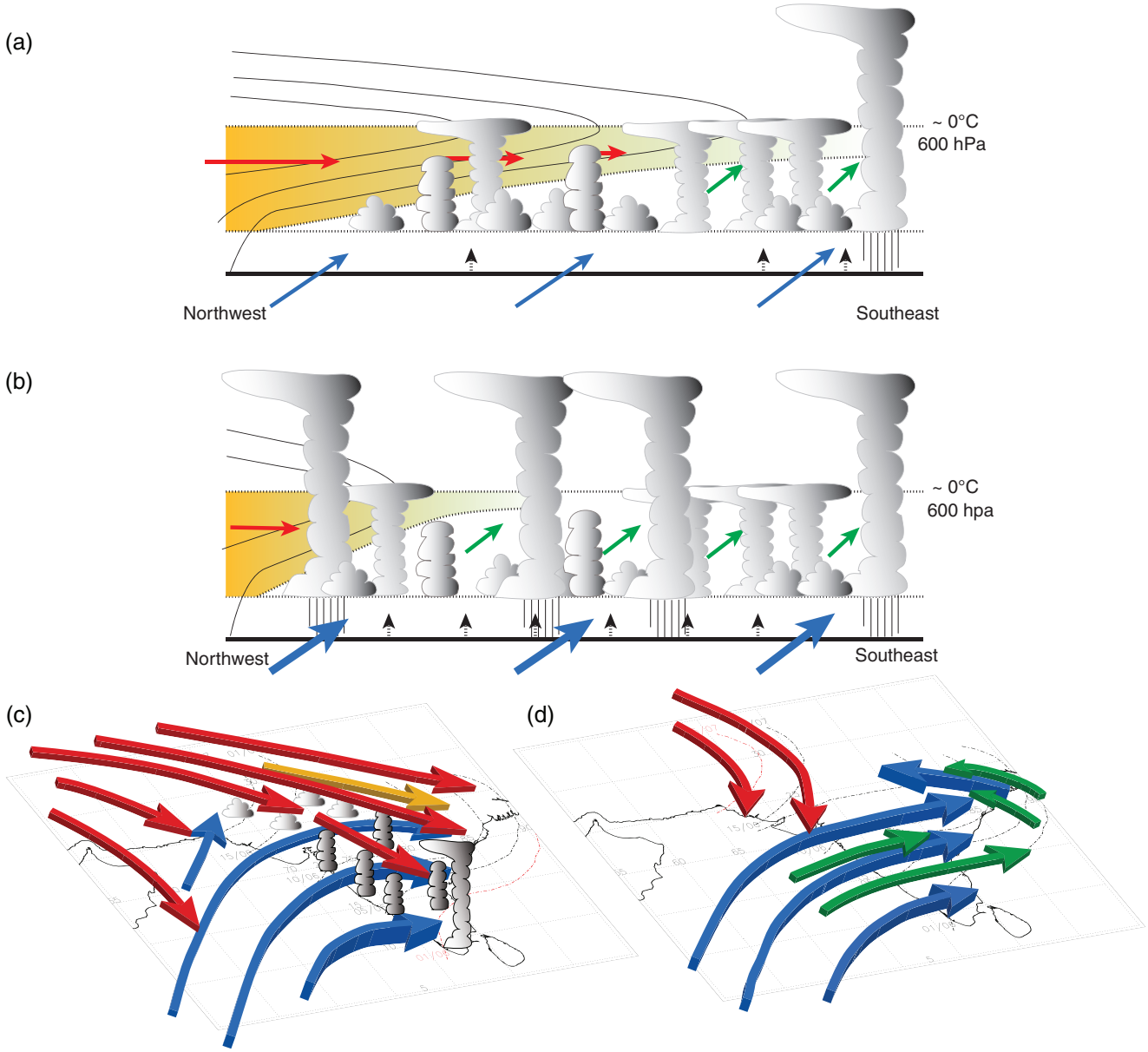

Figure 13. Schematic diagram encapsulating the conclusions drawn from data shown in the article. Panels (a) and (c) show the situation around the time of onset at Kerala (around 1 June) when the dry layer is still quite deep in the southeast, but has been sufficiently moistened to allow sustaining the onset of deep convection there. Panels (b) and (d) show the situation of around 15 July when the onset has moved to the northwest, and the dry layer extends only a few hundred kilometres into the subcontinent. (a) and (b) represent an approximately northwest to southeast vertical section in which contours of low equivalent potential temperature are denoted by fine lines, vectors indicate the horizontal wind vector in each layer, and black dotted arrows at the surface indicate evaporative fluxes, increasing between (a) and (b). The orange-shaded region shows the elevated residual mixed layer of low static stability advected from the northwest; the lower part of this layer is dry and warm, so it tends to suppress cumulus clouds. Panels (c) and (d) attempt to represent the flow in three dimensions, with the low-level flow (blue and orange arrows) undercutting mid-level dry (red) and moist (green) airflow. Typical clouds are represented in (c), but the more extensive cloud cover in (d) is omitted for clarity.

contributes to cyclonic curvature of the airflow (Figure 2(l)). We can also expect the mixing in the heat-low to yield very low potential vorticity (PV) in the levels below 600 hPa, and the subsequent advection of this low PV over India may play a role in delaying the development of the monsoon trough associated with the northern limit of the rains. Unfortunately, investigation of such dynamical feedbacks is beyond the scope of this study.

A further implication of this study is that the dry intrusion may play a role in the occurrence of early and late onsets of the monsoon at individual locations across India. Comprehensive study of the interannual variability will be a substantial challenge, beyond the scope of this article, because the establishment of a vertical profile suitable for onset of rain depends on the relative contributions of the monsoon flow, the dry layer and the land surface, each of which may have different characteristics in a given year. However, Figure 12 illustrates some evidence of systematic changes in the trajectory characteristics of the mid-level air, between years of late and early onset at Nagpur. Years in which the onset was late at Nagpur (Figure 12(a) and (c)) are often characterised by mid-level air which has descended from the northwest in the days before the onset. Years of early onset at Nagpur (Figure 12(b) and (d)) are more likely to exhibit back-trajectories emerging from oceanic regions, from lower altitudes, and which have typically moved more slowly over land.

This interpretation of the dynamics of monsoon onset provides an impetus for future study into the role of mid-level circulations and cloud–dynamical interactions, as well as the contribution of the land surface to these interactions. One may recall that the current generation of coupled GCMs simulate onsets that are too late, with poorly simulated progression (Sperber *et al.*, 2013). If, as argued here, the pattern of rainfall is controlled by the mid-level dry layer and its rate of moistening by shallow and congestus clouds, then models need to represent the shallow cumulus and congestus moisture, heat and momentum transports accurately, if they are to faithfully capture monsoon onset. The associated shallow and medium-level convective parametrizations are challenging for the models, which struggle in capturing the

evolution from shallow to deep convection. Furthermore, if the land surface also plays a role in supplying the humidity necessary to sustain the shallow clouds, the pre-monsoon wetting of the surface by intermittent rainfall events and associated development of vegetation needs to be captured by models. Often, models with parametrized convection struggle to deliver deep convective rainfall in the high-inhibition environments characteristic of the pre-monsoon period, and we cannot expect these models to capture the organisation of convective rainfall which seems to be important in the vicinity of the northern limit of rain (Ramanathan and Banerjee, 1931; Houze *et al.,* 2007; Romatschke and Houze, 2010; Krishnamurti *et al.,* 2012). We argue that in order to evaluate and improve the representation of shallow, medium and deep cumulus representations in the models, intensive observations of the cloud and dynamical fields around the period of the monsoon onset are required, including high-frequency (3 hourly) radiosondes, surface energy balance measurements, and cloud observations.

6. Conclusions

It is argued here that mid-level humidity is an important control on the local onset of monsoon rains. Consideration of the mid-level humidity can explain the progression of the monsoon onset, in terms of the movement of the northern limit of the rains from the south to the northwest, at right angles to or even upwind relative to the ambient flow in the lower troposphere.

As a result of the arguments contained in this article, we propose a new summary of monsoon onset dynamics and thermodynamics, illustrated schematically in Figure 13. In the pre-monsoon period, CIN is too high and CAPE low (due to low boundary-layer θ_e), and the mid-levels too dry to support widespread deep convection. As the onset proceeds:

I. Low-level westerly monsoon winds strengthen and deliver low-level moisture to the hot, dry continent.
II. The mid-level dry layer, carried by northwesterly winds, continues to suppress convection in the northwest. As the mid-level air flows towards the southeast, it is eroded from below by shallow cumulus and congestus (Figure 13(a) and (c)). Therefore the profile which is closest to pseudoadiabatic, with weakest inhibition of convection by CIN or lower-tropospheric dryness, is in the far southeast. There is a little rain in places, but in May everywhere it is still too dry for significant widespread rain. Occasional cumulonimbus events north of the northern limit are likely to deplete θ_e in the monsoon layer, through downdraughts.
III. Increasing and deepening low-level southwesterly monsoon winds increase the efficiency and rate of shallow-cumulus moistening (late May). Both over the Arabian Sea and over the land, the dry intrusion is progressively moistened from below as it moves to the southeast and, eventually, the first significant rains break out in the far south, where there is the least inhibition of moist convection (and no doubt enhanced by triggering over the Western Ghats).
IV. Increasing westerly monsoon winds continue to increase the efficiency and rate of shallow-cumulus moistening, meaning that everywhere the dry air is more strongly moistened from below, and the northern limit of rains shifts towards the northwest.
V. As the surface is made wet by rain, both ahead of and behind the northern limit of rains, the low-level air becomes progressively cooler and more humid. Equivalent potential temperature increases (with less entrainment of low θ_e from above), again favouring rain.
VI. The northwesterly mid-level flow weakens to the south of the northern limit of the monsoon due to mixing of momentum by deep convection, and to the intensification of the trough at this location, due to the moist convective heating (Raju *et al.,* 2005). In the deep convective zone, winds become more westerly through a deeper layer. Trajectories at 600 hPa mostly originate over the Arabian Sea at low levels. The weakening of the midlevel northwesterlies is also related to development of the anticyclone over the Himalayas, and the increasing easterly thermal wind, in relation to warm air to the north. By 15 July the dry layer has retreated to the far northwest, and the vertical section (Figure 13(b)) is as shown by Sawyer (1947) and Houze *et al.* (2007). In the northwestern region, the dry mid-level air contributes to very intense, organised storms. In the meantime, the strengthening monsoon trough has brought low-level and mid-level southeasterly winds into the far northeast of the subcontinent (Figure 13(d)).

The novelty of this interpretation is in emphasising the role of the mid-level dry air in preventing earlier onset (given that low-level monsoon moist advection is already robust in May) and in emphasising the role of cumulus and congestus clouds to the north of the northern limit of rains, in establishing the conditions needed for deep convection and the evolving location of the northern limit of the monsoon. The extent to which changes in the dry mid-level advection from the northwest are caused by cloud thermodynamic forcing (including cloud momentum transport retarding the northwesterly flow, and cloud heating modifying the circulation), or by larger-scale circulation changes (e.g. driven by thermodynamic changes over the Himalayas) remains to be seen. However, Bollasina and Ming (2013), in showing that onset proceeds in GCM experiments run in 'perpetual May' forcing, hints that the changing conditions allowing the onset of rains over India are in some sense 'internal' to the system rather than being imposed by changing large-scale forcing. In order to fully explain and quantify the relative roles of large-scale advection, cumulus moisture transport, precipitation and land-surface processes, more detailed analysis of these processes will be needed, including observations and high-resolution numerical simulation.

Acknowledgements

Parker, Marsham and Turner were supported by the INCOMPASS project (NERC NE/L013843/1 and NE/L01386X/1). Willetts is supported by a NERC PhD scholarship (NE/K006932/1; Met Office CASE) and Martin was supported by the Joint UK DECC/Defra Met Office Hadley Centre Climate Programme (GA01101). Interpolated OLR data were provided by the NOAA/OAR/ESRL PSD, Boulder, CO, USA, from their web site at http://www.esrl.noaa.gov/psd. Thanks to the British Atmospheric Data Centre, which is part of the NERC National Centre for Atmospheric Science (NCAS), for the calculation of trajectories and access to ECMWF data. We are indebted to Ashis Mitra and GS Bhat for useful suggestions, to Jim Galvin for discussion of the synoptic codes and remarks on forecasting practice, and to E. N. Rajagopal and J. P. Gupta for assistance with the local Nagpur and Lucknow onset dates.

References

Bartalis Z, Wagner W, Naeimi V, Hasenauer S, Scipal K, Bonekamp H, Figa J, Anderson C. 2007. Initial soil moisture retrievals from the METOP-A Advanced Scatterometer (ASCAT). *Geophys. Res. Lett.* **34**: L20401, doi: 10.1029/2007GL031088.

Betts AK. 1986. A new convective adjustment scheme. I: Observational and theoretical basis. *Q. J. R. Meteorol. Soc.* **112**: 677–692, doi: 10.1256/smsqj.47306.

Betts AK, Ball JH. 1995. The FIFE surface diurnal cycle climate. *J. Geophys. Res.* **100**: 25679–25693.

Bhat GS. 2006. The Indian drought of 2002 – a sub-seasonal phenomenon? *Q. J. R. Meteorol. Soc.* **132**: 2583–2602, doi: 10.1256/qj.05.13.

Bollasina MA, Ming Y. 2013. The role of land-surface processes in modulating the Indian monsoon annual cycle. *Clim. Dyn.* **41**: 2497–2509, doi: 10.1007/s00382-012-1634-3.

Boos WR, Kuang Z. 2010. Dominant control of the South Asian monsoon by orographic insulation versus plateau heating. *Nature* **463**: 218–222, doi: 10.1038/nature08707.

Carlson TN. 1998. *Mid-Latitude Weather Systems*. American Meteorological Society: Boston.

Chakraborty A, Nanjundiah RS, Srinivasan J. 2006. Theoretical aspects of the onset of Indian summer monsoon from perturbed orography simulations in a GCM. *Ann. Geophys.* **24**: 2075–2089.

Choudhury AD, Krishnan R. 2011. Dynamical response of the south Asian monsoon trough to latent heating from stratiform and convective precipitation. *J. Atmos. Sci.* **68**: 1347–1363, doi: 10.1175/2011JAS3705.1.

Dee DP, Uppala SM, Simmons AJ, Berrisford P, Poli P, Kobayashi S, Andrae U, Balmaseda MA, Balsamo G, Bauer P, Bechtold P, Beljaars ACM, van de Berg L, Bidlot J, Bormann N, Delsol C, Dragani R, Fuentes M, Geer AJ, Haimberger L, Healy SB, Hersbach H, Hólm EV, Isaksen L, Kållberg P, Köhler M, Matricardi M, McNally AP, Monge-Sanz BM, Morcrette J-J, Park B-K, Peubey C, de Rosnay P, Tavolato C, Thépaut J-N, Vitart F. 2011. The ERA-Interim reanalysis: Configuration and performance of the data assimilation system. *Q. J. R. Meteorol. Soc.* **137**: 553–597, doi: 10.1002/qj.828.

Dimri AP, Niyogi D, Barros AP, Ridley J, Mohanty UC, Yasunari T, Sikka DR. 2015. Western disturbances: A review. *Rev. Geophys* **53**: 225–246, doi: 10.1002/2014RG000460.

Fink AH, Agusti-Panareda A, Parker DJ, Lafore JP, Ngamini JB, Afiesimama E, Beljaars A, Bock O, Christoph M, Dide F, Faccani C, Fourrie N, Karbou F, Polcher J, Mumba Z, Nuret M, Pohle S, Rabier F, Tompkins AM, Wilson G. 2011. Operational meteorology in West Africa: observational networks, weather analysis and forecasting. *Atmos. Sci. Lett.* **12**: 135–141, doi: 10.1002/asl.324.

Galvin JFR. 2009. The weather and climate of the Tropics: Part 8 – Mesoscale weather systems. *Weather* **64**: 32–38.

Houze RA Jr, Wilton DC, Smull BF. 2007. Monsoon convection in the Himalayan region as seen by the TRMM precipitation radar. *Q. J. R. Meteorol. Soc.* **133**: 1389–1411, doi: 10.1002/qj.106.

Johnson RH, Ciesielski PE, Hart KA. 1996. Tropical inversions near the 0 degrees C level. *J. Atmos. Sci.* **53**: 1838–1855.

Joseph PV, Srinivasan J. 1999. Rossby waves in May and the Indian summer monsoon rainfall. *Tellus* **51A**: 854–864.

Ju J, Slingo JM. 1995. The Asian summer monsoon and ENSO. *Q. J. R. Meteorol. Soc.* **121**: 1133–1168.

Krishnamurthy V, Shukla J. 2000. Intraseasonal and interannual variability of rainfall over India. *J. Clim.* **13**: 4366–4377.

Krishnamurti TN, Thomas A, Simon A, Kumar V. 2010. Desert air incursions, an overlooked aspect, for the dry spells of the Indian summer monsoon. *J. Atmos. Sci.* **67**: 3423–3441, doi: 10.1175/2010JAS3440.1.

Krishnamurti TN, Simon A, Thomas A, Mishra A. 2012. Modeling of forecast model sensitivity on the march of monsoon isochrones from Kerala to New Delhi: The first 25 days. *J. Atmos. Sci.* **69**: 2465–2487.

Levine RC, Turner AG. 2012. Dependence of Indian monsoon rainfall on moisture fluxes across the Arabian Sea and the impact of coupled model sea surface temperature biases. *Clim. Dyn.* **38**: 2167–2190.

Levine RC, Turner AG, Marathayil D, Martin GM. 2013. The role of northern Arabian Sea surface temperature biases in CMIP5 model simulations and future projections of Indian summer monsoon rainfall. *Clim. Dyn.* **41**: 155–172.

Li CF, Yanai M. 1996. The onset and interannual variability of the Asian summer monsoon in relation to land sea thermal contrast. *J. Clim.* **9**: 358–375, doi: 10.1175/1520-0442(1996)009<0358:TOAIVO>2.0.CO;2.

Liebmann B, Smith CA. 1996. Description of a complete (interpolated) outgoing longwave radiation dataset. *Bull. Am. Meteorol. Soc.* **77**: 1275–1277.

Liu BQ, Liu YM, Wu GX, Yan JH, He JH, Ren SL. 2014. Asian summer monsoon onset barrier and its formation mechanism. *Clim. Dyn.* **45**: 711–726, doi: 10.1007/s00382-014-2296-0.

Mapes BE, Zuidema P. 1996. Radiative–dynamical consequences of dry tongues in the tropical troposphere. *J. Atmos. Sci.* **53**: 620–638, doi: 10.1175/1520-0469(1996)053<0620:RDCODT>2.0.CO;2.

Marathayil D, Turner AG, Shaffrey LC, Levine RC. 2013. Systematic winter sea-surface temperature biases in the northern Arabian Sea in HiGEM and the CMIP3 models. *Environ. Res. Lett.* **8**: 014028, doi: 10.1088/1748-9326/8/1/014028.

Marsham JH, Hobby M, Allen CJT, Banks JR, Bart M, Brooks BJ, Cavazos-Guerra C, Engelstaedter S, Gascoyne M, Lima AR, Martins JV, McQuaid JB, O'Leary A, Ouchene B, Ouladichir A, Parker DJ, Saci A, Salah-Ferroudj M, Todd MC, Washington R. 2013. Meteorology and dust in the central Sahara: Observations from Fennec supersite-1 during the June 2011 Intensive Observation Period. *J. Geophys. Res. Atmos.* **118**: 4069–4089, doi: 10.1002/jgrd.50211.

Moron V, Robertson AW. 2014. Interannual variability of Indian summer monsoon rainfall onset date at local scale. *Int. J. Climatol.* **34**: 1050–1061.

Nandankar PK, Dewangan PL, Surpam RV. 2011. *Climate of Nagpur*. India Meteorological Department: Nagpur. http://imdnagpur.gov.in/Climate_NGP.pdf (accessed 29 March 2016).

Pai DS, Bhan SC. 2014. 'Monsoon 2014: a report'. IMD Met. Monograph: ESSO Document No.: ESSO/IMD/SYNOPTIC MET/01(2015)/17. http://www.imd.gov.in/section/nhac/dynamic/monsoon_report_2014.pdf (accessed 29 March 2016).

Pai DS, Bhate J, Sreejith OP, Hatwar HR. 2011. Impact of MJO on the intraseasonal variation of summer monsoon rainfall over India. *Clim. Dyn.* **36**: 41–55.

Parker DJ, Thorncroft CD, Burton RR, Diongue-Niang A. 2005. Analysis of the African easterly jet, using aircraft observations from the JET2000 experiment. *Q. J. R. Meteorol. Soc.* **131**: 1461–1482.

Parsons DB, Yoneyama K, Redelsperger JL. 2000. The evolution of the tropical western Pacific atmosphere–ocean system following the arrival of a dry intrusion. *Q. J. R. Meteorol. Soc.* **126**: 517–548, doi: 10.1256/smsqj.56306.

Prakash S, Mitra AK, Momin IM, Rajagopal EN, Basu S, Collins M, Turner AG, AchutoRao K, Ashok K. 2015. Seasonal intercomparison of observational rainfall datasets over India during the southwest monsoon season. *Int. J. Climatol.* **35**: 2326–2338, doi: 10.1002/joc.4129.

Raju PVS, Mohanty UC, Bhatla R. 2005. Onset characteristics of the southwest monsoon over India. *Int. J. Climatol.* **25**: 167–182, doi: 10.1002/joc.1121.

Ramanathan KR, Banerjee HC. 1931. A study of two pre-monsoon storms in the Bay of Bengal and a comparison of their structure with that of the Bay storms in the winter months. *Sci. Notes India Met. Dep. Calcutta* **4**: 34.

Romatschke U, Houze RA. 2010. Regional, seasonal, and diurnal variations of extreme convection in the South Asian region. *J. Clim.* **23**: 419–439, doi: 10.1175/2009JCLI3140.1.

Sabin TP, Krishnan R, Ghattas J, Denvil S, Dufresne J-L, Hourdin F, Pascal T. 2013. High resolution simulation of the South Asian monsoon using a variable resolution global climate model. *Clim. Dyn.* **41**: 173–194, doi: 10.1007/s00382-012-1658-8.

Saith N, Slingo J. 2006. The role of the Madden–Julian Oscillation in the El Niño and Indian drought of 2002. *Int. J. Climatol.* **26**: 1361–1378.

Sandeep S, Ajayamohan RS. 2014. Origin of cold bias over the Arabian Sea in climate models. *Sci. Rep.* **4**: 6403, doi: 10.1038/srep06403.

Sawyer JS. 1947. The structure of the intertropical front over N.W. India during the S.W. Monsoon. *Q. J. R. Meteorol. Soc.* **69**: 346–369.

Sperber KR, Annamalai H, Kang I-S, Kitoh A, Moise A, Turner AG, Wang B, Zhou T. 2013. The Asian summer monsoon: An intercomparison of CMIP5 vs. CMIP3 simulations of the late 20th century. *Clim. Dyn.* **41**: 2711–2744.

Tuinenburg OA, Hutjes RWA, Kabat P. 2012. The fate of evaporated water from the Ganges basin. *J. Geophys. Res. Atmos.* **117**: D01107, doi: 10.1029/2011JD016221.

Wheeler MC, Hendon HH. 2004. An all-season real-time multivariate MJO index: Development of an index for monitoring and prediction. *Mon. Weather Rev.* **132**: 1917–1932.

Wu G, Zhang Y. 1998. Tibetan Plateau forcing and the timing of the monsoon onset over South Asia and the South China Sea. *Mon. Weather Rev.* **126**: 913–927.

Wu G, Liu Y, Wang T, Wan R, Liu X, Li W, Wang Z, Zhang Q, Duan A, Liang X. 2007. The influence of mechanical and thermal forcing by the Tibetan Plateau on Asian climate. *J. Hydrometeorol.* **8**: 770–789, doi: 10.1175/JHM609.1.

Wu G, Liu Y, He B, Bao Q, Duan A, Jin F-F. 2012a. Thermal controls on the Asian summer monsoon. *Nat. Sci. Rep.* **2**: 404, doi: 10.1038/srep00404.

Wu G, Guan Y, Liu Y, Yan J, Mao J. 2012b. Air–sea interaction and formation of the Asian summer monsoon onset vortex over the Bay of Bengal. *Clim. Dyn.* **38**: 261–279, doi: 10.1007/s00382-010-0978-9.

Xavier PK, Marzin C, Goswami BN. 2007. An objective definition of the Indian summer monsoon season and a new perspective on the ENSO–monsoon relationship. *Q. J. R. Meteorol. Soc.* **133**: 749–764, doi: 10.1002/qj.45.

Yatagai A, Kamiguchi K, Arakawa O, Hamada A, Yasutomi N, Kitoh A. 2012. APHRODITE: Constructing a long-term daily gridded precipitation dataset for Asia based on a dense network of rain gauges. *Bull. Am. Meteorol. Soc.* **77**: 1275–1277, doi: 10.1175/BAMS-D-11-00122.1.